Lappeenranta University of Technology
School of Engineering Science
Computational Engineering and Technical Physics
Technical Physics

Valeriia Baranauskaite

STRUCTURAL AND INTERPARTICLE INTERACTIONS IN THE MODEL SYSTEMS OF NATURAL BRINES

Master's Thesis

Examiners: Professor Erkki Lähderanta

Supervisors: Associate Professor Olga Pestova

ABSTRACT

Lappeenranta University of Technology
School of Engineering Science
Computational Engineering and Technical Physics
Technical Physics

Valeriia Baranauskaite

Structural and interparticle interactions in the model systems of natural brines

Master's Thesis

2019

69 pages, 49 figures, 17 tables.

Examiners: Professor Erkki Lähderanta

Keywords: Nuclear Magnetic Relaxation, brines, water-based multicomponent systems, solutions

This study is dedicated to dynamics and structures of the water-based multicomponent solutions studied at wide temperature and concentration ranges. Since the scientific interest towards aqueous solutions has been shared by many scientists: physics, chemists, biologists and even mathematicians, there are many speculations about micro properties of water-based systems. As for today, there are no wide spread models and theories about structure of water-based solutions. In this study the use of phenomenological model of concentrated electrolyte solutions structure is presented. The systematic approach was used to study three ternary water-based systems. Eutectic concentrations of ternary solutions were determined with cryoscopic measurements. NMR measurement were conducted for solutions, and possible ionic surrounding was described. The standard formation enthalpies of double salts were calculated with help of calorimetric studies. The structural properties of double salts obtained from X-ray experiments were discussed. These results are necessary for further Molecular Dynamical computations.

PREFACE

I would like to thank my supervisor Olga Pestova, scientific advisers Andrey Efimov and Vladimir Matveev for fruitful discussions and precious comments.

Valeriia Baranauskaite

CONTENTS

1 Introduction **6**
1.1 Background . . . 6
1.2 Objectives and delimitations . . . 8

2 Literature Review **9**
2.1 Views and models of the structure of liquid water . . . 10
2.2 The structure of electrolyte solutions . . . 11
2.3 Mechanisms of formation of a solid phase from multicomponent solutions 13
2.4 Some items of the theory of Nuclear Magnetic Relaxation . . . 13
2.5 Measurement of Self-Diffusion coefficient . . . 15
2.6 Thermodynamic studies of solutions . . . 17

3 Experiment details **18**
3.1 Samples . . . 18
3.2 Cryoscopy experiment . . . 19
3.3 NMR experiment details . . . 20
3.4 X-ray crystallography and Powder diffraction . . . 20
3.5 Calorimetry experiment . . . 21

4 Results and discussion **23**
4.1 X-Ray . . . 29
4.1.1 $MgCl_2 \cdot CsCl \cdot 6\,H_2O$ . . . 29
4.1.2 $MgCl_2 \cdot LiCl \cdot 7\,H_2O$ . . . 31
4.1.3 $LiCl \cdot 3\,CsCl \cdot 4\,H_2O$ . . . 34
4.1.4 $4\,LiCl \cdot 3\,CsCl \cdot 2\,H_2O$ . . . 37
4.2 Powder diffraction . . . 47
4.3 Calorimetric measurements . . . 48
4.3.1 $MgCl_2 \cdot CsCl \cdot 6\,H_2O$ . . . 49
4.3.2 $MgCl_2 \cdot LiCl \cdot 7\,H_2O$ . . . 51
4.3.3 $LiCl \cdot 3\,CsCl \cdot 4\,H_2O$ . . . 53
4.4 NMR . . . 56
4.4.1 Spectroscopy . . . 56
4.4.2 Self-diffusion of water molecules . . . 56
4.4.3 Longitudinal relaxation times T_1 . . . 61

5 Conclusions **64**

REFERENCES **64**

LIST OF ABBREVIATIONS

CG	Cybotactic group
NMR	Nuclear Magnetic Relaxation
PFG	Pulsed Magnetic Field Gradient
QCC	Quadrupole coupling constant
XRC	X-ray crystallography

1 Introduction

1.1 Background

Water covers approximately 71% of the Earth surface, it is essential for many branches of human activities. Humanity and other life forms depend on the liquid water, on its purity and abundance. Thus water has been a subject of interest for many scientists through the centuries. Naturally, water always includes impurities: inorganic salts, organic compounds, micro biological systems, the latent and pronounced properties of water would depend strongly on the composition and concentration of impurities [1].

Water-based electrolyte solutions among other liquid systems have drew a lot of researchers' attention due to their wide use in the different chemical, biological and technological processes [2–5]. Binary systems have been studied far and wide, their individual parameters are written in textbooks and handbooks [6]. However there is a lack of information and experiments for multicomponent systems, which occupy a huge niche among other liquid systems. Previous research efforts were often focused on simple binary water-based systems or molten multicomponent systems. Absence of studies upon ternary systems is connected with complexity of these objects, lack of phase diagrams. Studies of ternary systems require systematic approach with many methods involved. Multicomponent water-based electrolyte solutions are present at high concentrations in natural brines. These solutions have a huge field with vast literature and applications varying from the removal desalination of water in the natural environment to eco-friendly energy sources and refrigerants [7]. These applications are based on thermophysical and dynamical characteristics of systems over wide ranges of temperature, pressure and concentration. Prediction and modeling of suitable macro properties can be made with help of Molecular Dynamics and Quantum Chemistry. These methods also rely on many models and theories about structure and interactions in the systems. Structure and interactions are key parameters for the multicomponent electrolyte solutions, these are enough to describe complex and fickle systems with strict *ab-initio* methods. Structure of water-based electrolyte solutions and state of the water molecules are still doubtful, there is still a lack of solubility diagrams able to depict real systems.

Whereas the known regularities and models for the diluted solutions could be successfully applied for the low- or moderate-concentrated solutions thanks to correcting factors, the same laws are not applicable for highly concentrated solutions [8]. The phenomenological model of the structure of the concentrated electrolyte solutions is used for results interpretation. It is, *a priori*, possible to interpret experimental results and to describe

the influence of ions on these properties using two basic ideas: the Samoilov theory and the idea of similarity of the solid phase structure which crystallizes from the solution and structure of the cybotactic group (dominant structure of the solution).

As for today, there are no wide spread models and theories about structures of liquid water-based electrolyte solutions. Many industrial calculation and predictions are based on the semi-empirical methods with coefficients distinct for each particular system. Industrial applications and use of concentrated electrolyte solutions include salting out pure components from a mixture, electrolysis, use as reagents or solvents in chemical reactions. Such systems are used, in particular, as refrigerants thanks to their low freezing temperatures, they are also environmentally friendly, reusable and do not require additional maintenance for disposal. Purification techniques (salting out and crystallization) are based on different solubilities of solid salts in the multicomponent systems. These methods rely on the properties of highly concentrated solutions (polythermal crystallization) or evaporation of the solvent at a constant temperature (isothermal crystallization). The solubility strongly depends on the temperature for the vast majority of compounds, the decrease of solubility naturally responds on the temperature decrease. Polythermal crystallization method is used for such systems. In this method a hot saturated salt solution is cooled down, producing supersaturation in solution, which causes crystallization, and the amount of the solvent does not change. In case of isothermal crystallization, the supersaturation of the solution is achieved by the solvent removing at a constant temperature corresponding to the boiling point of the solvent. The additional components, which lower target salt solubility, are called salting out agents, they have the same ion with the target salt. Also organic solvents are additionally used to increase the efficiency of the process [9].

All of the forementioned methods require knowledge of the phase diagrams, mixed and individual solubilities. Thermodynamics give more detailed representation about the ease and rate of these processes, but as a macro parameter it can't help to interpret and understand micro evolution and dynamics. Thereby a lot of methods are needed to determine the liquid system parameters.

All the solutions can be divided into three groups: diluted, eutectic and concentrated. In the diluted solutions the structural dominant is solvent, and the structural parameters (coordination numbers of ions, type and amount of ionic pairs) are dictated by solvent. In the concentrated solutions the structural dominant changes from the solvent (i.e. water) to the salt, and the salt will attempt to build its own structure. The eutectic solution is known for its chaotic structure and entropy maximum, there is a structural micro-heterogenity which would influence such properties as freezing temperature. At eutectic concentration

solution would have the lowest freezing temperature. The structure of the multicomponent concentrated electrolyte solution would be determined by the structural dominant called cybotactic group. The cybotactic groups have been described in [10, 11] as structural associates, spatial mean particles ordering in post-eutectic solutions. The composition of cybotactic group is dictated by the composition of the solid phase crystallizing from the solution with temperature decrease.

1.2 Objectives and delimitations

The goal of this research is to define the mutual ions influence in the set of multicomponent electrolyte solutions with alkali cations with help of systematic approach.

This goal will be met by achieving the following objectives

1. To synthesize double-salts crystals from solutions, determine their phases and compositions
2. To measure freezing temperatures of solutions for the wide concentration range
3. To measure structural-dynamical T_1 and energetic E_{act} characteristics in wide concentration and temperature ranges
4. To measure Self-diffusion coefficient for each nuclei in wide concentration and temperature ranges
5. To measure dissolution enthalpies of double salts and of binary salts mix

2 Literature Review

Water is a simple compound but due to its structure it has specific properties. It is known that the physical and chemical properties of water as a solvent differ sharply from other solvents, as well as from the properties of other hydrides of the 16th group elements and the second period of periodic system.

Figure 1 shows the hydride boiling points. As it can be seen from this figure, for the elements N, F and O from the second period, the boiling points are higher than expected, and for water it is maximum [12]. In addition to boiling temperatures, water can also be distinguished by the fact that its liquid phase is denser than solid, it can be supercooled by more than $40°C$, and decrease in volume during subsequent heating to $4°C$, where its density is maximum.

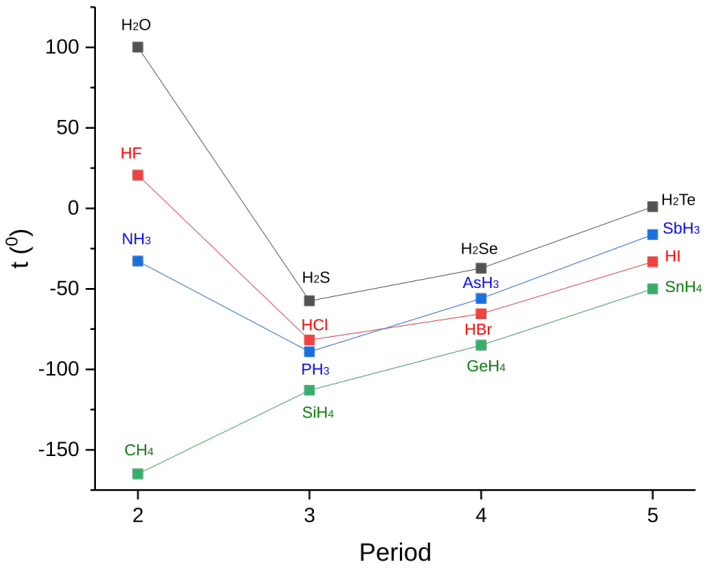

Figure 1. Boiling points of hydrides of elements of the main subgroups of 1-5 periods [12].

Directed hydrogen bonds in water have a large energy (5 kcal/mol), compared with Van der Waals interactions, due to electro-static and donor-acceptor interactions. It is assumed that hydrogen bonds bind from 3 to 50 water molecules in associates. The water molecule has 4 charged centers: 2 positively charged hydrogen, and two negatively charged lone electron electron pairs. Electrostatic interactions occur between oppositely charged centers, with the formation of a tetrahedron, similar to that which exists in the crystal structure of ice [13]. Since the hydrogen ionization energy is the lowest among all the elements, its electron easily shifts towards oxygen, while hydrogen acquires a partial positive charge

δ^+, excess electron density accumulates on oxygen, and it acquires a partial negative charge δ^-. The bond is polarized and favorable conditions are created for the protons exchange between oxygen atoms and autoprotolysis with the formation of hydroxyl ion. A characteristic feature of the hydrogen bond is the chain-like character of formation (interference effect) and the formation of one hydrogen bond causes the formation of new hydrogen bonds by an avalanche. Moreover, in the liquid state, water molecules are mobile and perform rotational-oscillatory motions, which can be determined with spectroscopic methods, Brownian motion of water molecules, chaotic and directed jumps are also observed. Movements of water molecules cause the destruction and the emergence of hydrogen bonds along with micro-heterogeneity of the structure, a constant change in the distances between molecules. Since all movements are random, fluctuations of average density and average orientation are statistical by nature [14].

2.1 Views and models of the structure of liquid water

The hydrogen bond characteristics described above define unique water properties and features of water structure. Some physical and chemical properties are macro properties that can be measured, but the structure of liquid water is a micro property and can't be directly determined. Calculated density of water, under the condition that water molecules are spherical, exceeds experimental density values. This indicates the presence of inhomogeneities of lower density. Many contradictory and complementary hypotheses and models explaining the anomalous properties of liquid water have been created, attempts to prove these theories have been made so far. Different areas with uneven density were represented as water molecules associated with hydrogen bonds and some monomers. The monomers could be hindered by the inside of the associates, or placed outside, depending on the model. Many theories for the moment are based on the two facts: hydrogen bonds are arranged in liquid water like in a solid phase, or like in a gaseous phase. The first theory was voiced by X-rays, which suggested the structural heterogeneity in liquid water. The second theory was expressed by Bernal and Fowler, it was based on ice structure data known by that time. They assumed that in a liquid, as in ice, water remains in a form of tetrahedron, a solid-liquid phase transition manifests itself in the crystal structure change. Pseudocrystalline structure of water depends on the temperature, for example, at $4^{\circ}C$, the structure of water is similar to the structure of ice. Samoilov, on the basis of these theories, suggested that the structure of water is similar to the crystal structure of hexagonal ice, the same network of hydrogen bonds is preserved in it, and single water molecules are embedded inside the voids of the cages. With an increase in temperature from negative to $+40^{\circ}C$, the amount of such molecules increases until there are no free

voids for them. In fact, at $4°C$ the ratio of water molecules bound by hydrogen bonds is optimal.

To date, it has become possible to obtain data on the structure of water not only with the help of optical spectroscopy or X-ray diffraction, but also with the help of such a powerful and informative method as EXAFS (Extended X-Ray Absorption Fine Structure). Short-term shooting in this method allows one to capture instant structures even in liquid water. One can specify the Molecular Dynamics (MD) method and the Density Function Theory (DFT) in mathematical and computer methods for studying water. Now, the MD method lacks the ability to take into account the cooperativity of hydrogen bonds, and for DFT there is not enough computer power [15].

2.2 The structure of electrolyte solutions

As the salt dissolves in two-component electrolyte system, sequential structural changes occur in the solution as a whole. The whole concentration range can be divided into three areas: diluted solutions, medium concentration solutions and concentrated solutions (post-eutectic). In the diluted aqueous solutions the main dominant component is water which determines the physical-chemical characteristics of the system. For such systems the laws of ideal solutions are applicable with an acceptable error. In solutions of medium concentrations, the model of H. Frank, M. Ivens and V. Ven is used [16]. The solution is divided into three different structural zones or areas. In the first area, the ion has main influence on water molecules, it is called the ionic zone. In the second area there is water that does not have its own structure with a network of hydrogen bonds, nor a structure oriented relative to the ion, it is called a zone of degraded water. In the third area there is water with a characteristic structure of its own (Fig. 2) Ions, in turn, are divided into two types: positive and negative hydrated. Positively hydrated ions reduce water mobility, for example: Li^{+}, Mg^{2+}, Al^{3+}, F^{-},$SO_4{}^{2-}$. Negatively hydrated ions include ions that increase the mobility of water, for example: Cs^{+}, Tl^{+}, ClO^{4-}, I^{-}.

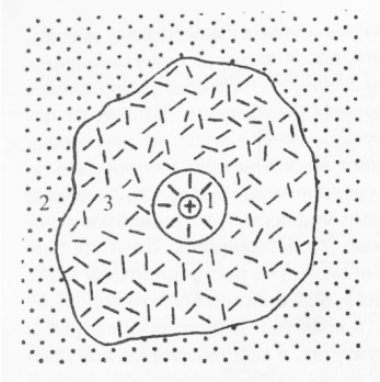

Figure 2. The band structure of electrolyte solutions.

Concentrated solutions include post-eutectic concentration solutions, where the structural dominant is no longer pure water, but a salt, since at high concentrations the water cannot build its own structure. The structural dominant is similar to a crystal that crystallizes out as the temperature decreases. As concentration of the dissolved substance increases, the temperature of formation of the solid phase decreases till the eutectic point. It is known that before the eutectic concentration, water crystallizes out of the solution because it is the solvent, the dominant compound. After reaching the eutectic concentration, the freezing temperature of the solution increases, and the dissolved substance crystallizes. This is due to a change in the structural dominant compound. At the eutectic point, water (ice) and a solute (anhydrous salt or crystalline hydrate) crystallize out of solution. Thus, it is clear that at some point, determined for each salt, roles change, and the water is already dissolved in the salt. The maximum entropy is also characteristic of the eutectic concentration range. It should be noted that water molecules will not be permanently a part of only the dissolved component or only part of the structural dominant. They will continuously change among themselves as it happens in the structure of water, therefore, in the experiment, where registration rate requires more time than the rate of exchange of water molecules, one will not observe strict separation of dissolved water and water, which is part of the structural dominant. The average state of the water between these two extremes can be determined with long registration time.

The definition of a concentrated solution by change in the structural dominant (and in fact, by the position of eutectic point on the solubility phase diagram) will be different for different salts. For example, the eutectic concentration may be at a small, average or large proportion of salt. In the first case, after the eutectic point, a stable crystalline hydrate is usually formed, and in the latter - anhydrous salt. After the eutectic concentration, the processes of structural-induced interaction become the main ones, and micro-heterogeneity appears. The structurally-ordered state is called a cybotactic, its structural units asso-

ciates consisting of water and salt – are called cybotactic groups (CG). A characteristic feature of cybotactic groups is that their structure corresponds to the structure of the solid phase, which crystallizes from solution upon cooling. This theory is a generalized phenomenological model of the structure of aqueous solutions of electrolytes, it has been confirmed by papers [17], [11].

2.3 Mechanisms of formation of a solid phase from multicomponent solutions

The process of double salt formation, according to [18], is called structurally induced complexing. This mechanism is carried out only at post-eutectic concentrations. The formation of double salt is not possible if CGs are structurally incompatible, incapable of forming a single communication system. In this case, the formation of microinhomogeneities will occur in the solution, but a joint compound will not be formed. In systems where the CGs are structurally compatible with each other, the formation of a double salt is possible and can occur in three ways. If the salts are the same by nature, double salt will be formed by the structurally induced conjugation mechanism. If the salts are different by nature, the formation of double salts will proceed according to the structurally induced substitution mechanism. The third option, applicable to salts of different nature, in which the ions cannot replace each other due to different sizes or other structural features, the resulting double salt will be of a layered structure formed by the structure-induced implantation mechanism. Solvated particles may exist in solutions that do not correspond to the solid phase that crystallizes from the solution. Salts, that are prone to complex formation or hydrolysis in solution, form a huge number of different forms of such solvated particles. Thus, several types of structural associates may exist in a solution,. However it is the one which is similar to the structure of the solid phase obviously more energy-efficient, and has longer living time. When the solution is concentrated, its structure and the corresponding dominant sub-structures, which are individual for each individual system, change sequentially.

2.4 Some items of the theory of Nuclear Magnetic Relaxation

Nuclear Magnetic Relaxation allows one to study environment of nuclei, which have a magnetic moment. In particular, the study of relaxation processes allows to determine structural and dynamical parameters associated with water molecules and ions mobility (relaxation times and activation energy). In NMR experiment macroscopic magnetization

is driven from equilibrium position at high frequency (at NMR scale) with electromagnetic impulse. The sample is placed in a constant magnetic field from 2 Tesla (NMR in a low field) up to 13 Tesla (high field NMR). The spin level of the magnetic nucleus splits with spin I into 2I + 1 component, the population of these levels is described by the Boltzmann distribution. In this distribution: n_i is a number of particles in certain state with energy E_i, k Boltzmann constant, T absolute temperature, A pre-exponential factor.

$$n_i = Ae^{-E_i/kT} \tag{1}$$

First, spin system is placed in the constant magnetic field to achieve "equilibrium" state according to Boltzmann distribution. Second, a short radio frequency impulse drives spins from equilibrium position. The frequency of short impulse is Larmor frequency, which is different for each nuclei, it corresponds in the energy scale to the energy difference of spin splitted levels.

$$\omega_0 = -\gamma H_0 \tag{2}$$

Where γ is the gyromagnetic ratio of the nuclei constituting the spin system. Thus, the system in a short time is driven from equilibrium state, the ensemble of spins absorbs energy of resonant radio frequency pulse. In a short time radio frequency (RF) pulse stops, and the system gradually comes back to equilibrium state (relaxation process) with Boltzmann distribution. Relaxation process has a characteristic time (relaxation time). Using different sequences of RF pulses it is possible to register spin-lattice (T_1) or spin-spin (T_2) relaxation times. In relaxation process spin system exchanges absorbed energy. The exchange may occur between spin and lattice (any form of molecular environment) due to fluctuations of magnetic fields or inside spin system. Fluctuations of magnetic fields appear as the result of the movement of particles inside the system. There are several relaxation mechanisms: dipole-dipole, scalar, spin-rotational, quadrupole and electron screening anisotropy of the nucleus.

In the systems under study, relaxation was recorded for the ^{133}Cs nucleus. Its spin $I = 7/2$, it has 78 neutrons and 55 protons. For this core there is a distribution of the charge carriers' displacement symmetry along the axis. And, since the sign of the electric quadrupole moment of the nucleus is a negative value, $-[0.3 - 3] \cdot 10^{-2}$ (barn), the spheroid of the nucleus is flattened towards the spin direction. ^2H nucleus has only one proton and one neutron, the spin of this nucleus is $I = 1$. It is also a quadrupole nucleus,

the electric moment of which is $2.8 \cdot 10^{-3}$ (barn), the positive value of the quadrupole moment indicates extended distribution of charge in the nucleus relative to the spin of the nucleus. If the electric field around quaprupole nucleus is asymmetrical and has a gradient then this electric field gradient will interact with the quadrupole moment of the nucleus. When electric field gradient fluctuates in time with a Larmor frequency, the excess energy transfers from the nucleus to the lattice. The electric field gradient will fluctuate with time, thanks to intramolecular movements, and since quadrupole relaxation has an effect on determined values of relaxation times and rates, then even the slightest change in the electric field symmetry will reflect on characteristic times. This method is applicable to liquid, solid and gaseous systems, to organic and inorganic compounds. A huge amount of papers is dedicated to NMR application in electrolyte solutions [19], [20], [21]. For example, in [22] the structure of the cation solvation shell was studied by NMR method. Authors state that the environment of the Ca^{2+} cation consists of two layers (water) with different molecular mobility. In the first layer calcium is surrounded by 6 water molecules, and in the second by 12. Coordination number is one of the most important characteristics of an ion in a solution; it gives representation of the dominating interactions in the inner solvation shell. NMR was also used in the work [23] to study the mobility of water molecules in zeolites. Authors managed to distinguish between different types of water molecules: water molecules in the main channel and in the side "pockets" or coordinated water molecules. They also managed to identify activation energies of water molecules diffusion process of intercrystallization and intracrystallization. According to the above-mentioned examples, NMR is used to study aqueous solutions for a very long time and is widespread, due to its tremendous capabilities.

2.5 Measurement of Self-Diffusion coefficient

Self diffusion is the process of the molecules chaotic thermal motion in a thermodynamically equilibrated medium. The self-diffusion measurement technique requires a specific sequence of RF pulses along with an applied magnetic field gradient. Such a technique is called NMR with a Pulsed Magnetic Field Gradient (PFG). This method captures the loss of spins phase coherence due to translational movements in the magnetic field gradient. The function of diffusion attenuation, from which information on diffusion processes is extracted, is a dependence of the spin echo signal amplitude on time and the magnetic field gradient. In turn, the spin echo amplitude depends on the molecules relaxation and translational motions. In NMR experiment with PFG, the system is exposed to a three-pulse sequence of stimulated echo (Fig. 3).

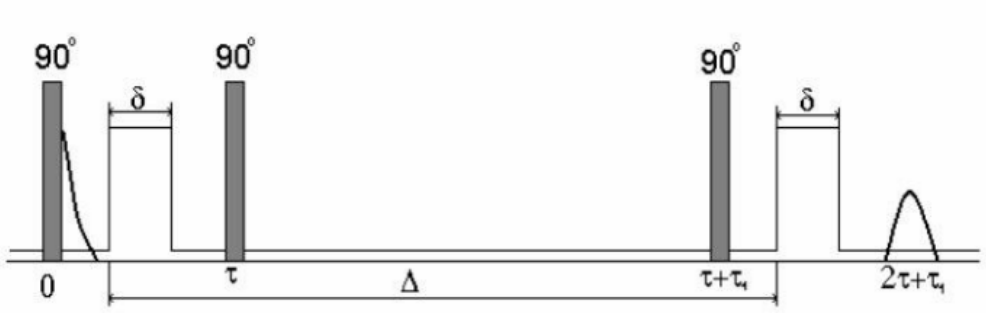

Figure 3. Three-pulse stimulated echo sequence.

In the stimulated echo technique, the expression for the amplitude $A(2\tau, \tau_1, g)$ of the echo is written as following

$$A(2\tau, \tau_1, g) = \frac{A(0)}{2} exp[-\frac{2\tau}{T_2} - \frac{\tau_1}{T_1}] exp[\gamma^2 g^2 \delta^2 t_d D_s (\Delta - \frac{\delta}{3})] \tag{3}$$

Where T_1 is longitudinal relaxation time, T_2 is transverse relaxation time, t_d is diffusion time, D_s is self-diffusion coefficient, g is gradient amplitude, γ is gyromagnetic ratio, δ is gradient duration, τ_1 is time delay between the second and third impulse, $A(0)$ is the echo amplitude in the beginning of sequence, Δ is delay between two gradients, τ is delay between the first and the second impulse.

This technique with a three-pulse sequence of stimulated echo is the most commonly used method of measuring the self-diffusion coefficients, since it eliminates the effects of relaxation time reduce. Figure 3 shows a three-pulse sequence of stimulated echo. In the absence of gradient pulses, this scheme will look like a standard spin-echo sequence, where the orientation of chemical shifts proceeds as if the signal was attenuated solely by transverse relaxation. In the presence of pulsed gradient field, the first gradient pulse creates a spatial vector magnetization dependence on the phase, and the magnetization vector can be reoriented by a second gradient pulse of the same magnitude and duration δ. A complete spin reorientation occurs only if the local field influence on the spin is absolutely the same for both gradient pulses. Since there is a gradient of magnetic field, this condition is observed only in cases when the molecules are not diffusing. If the molecules diffuse in time Δ, then the local fields applied by two pulses will not coincide and only partial reorientation will occur, and the detected signal will be reduced depending on the distance the molecules diffusion. The first 90-degree impulse superimposed on the system reverses the macroscopic magnetization vector so that it becomes transverse within

a short period of time τ (1-10 ms), the second 90-degree impulse reverses the magnetization vector so that it becomes longitudinal longitudinal relaxation is potentially longer than transverse. Under such conditions, the diffusion of molecules is measured with a longitudinal orientation of the macroscopic magnetization vector, with time τ_1 [24]. The information extracted using NMR PFG very accurately reflects the micro-properties of the systems. Unlimited diffusion during the selected time interval acquires the physical meaning of the mean square displacement in space. Moreover, the NMR PFG technique with Fourier transform is the only method to quantify self-diffusion of system components. Such data, for example, can serve for comparison with the values of self-diffusion coefficients obtained from theoretical calculations [25]. Self-diffusion coefficients are important parameters of ionic liquids, there is a large number of works devoted to these studies [26].

2.6 Thermodynamic studies of solutions

Thermodynamics of aqueous solutions is one of the most promising and necessary areas of solution chemistry as described in [27] and [28]. The calorimetry method used in this work allows to determine precise heat effects of processes and reactions. For example, with help of the literature data it is possible to calculate standard enthalpy of formation [29] or energy of the crystal lattice [30] using heat effect of dissolution. AS it was shown in [30] it is possible to calculate Pitzer coefficients from this data as well for further usage and calculations. The heat effect of dissolution represents interactions of ions with solvent [31]. It is useful for comparison with results of MD and DFT methods.

3 Experiment details

3.1 Samples

Pure reagents CsCl (ACS), $MgCl_2 \cdot 6\,H_2O$ (ACS), LiCl (ACS), D_2O (99.9%) were used in this study. Chlorides concentrations were determined by Mohr method, magnesium concentration was determined by complexometry titration method.

Solutions of $MgCl_2 - CsCl - H_2O$ system were prepared in the concentration ratio $Cs/Mg = 1.79 : 1$. The components are dry CsCl salt, $MgCl_2$ saturated solution, and distilled water. The calculated mass of CsCl was added to the saturated solution $MgCl_2$ with constant stirring, after that the solution was diluted to mark with H_2O. After that the solutions of lower concentrations were prepared by dilution method. These solutions were used in the NMR experiments (relaxation times measurements on nuclei ^{133}Cs; and self-diffusion for ^{1}H) and cryoscopy experiments. The total amount of samples was 5 and 10 for NMR and cryoscopy experiments respectively.

Solutions of $MgCl_2 - LiCl - H_2O$ system were prepared in the concentration ratio $Li/Mg = 7.03 : 1$. The components are LiCl saturated solution, $MgCl_2$ saturated solution, and distilled water. The saturated $MgCl_2$ and LiCl solutions were mixed in accordance to the calculated volume ratio. After that the solutions of lower concentrations were prepared by dilution method. These solutions were used in the NMR experiments (self-diffusion for ^{1}H nuclei) and cryoscopy experiments. The total amount of samples was 7 and 12 for NMR and cryoscopy experiments respectively.

Solutions of $LiCl - CsCl - H_2O$ system were prepared in the concentration ratio $Li/Cs = 2 : 1$. The components are LiCl saturated solution, CsCl dry salt, and distilled water. The calculated mass of CsCl was added to the saturated solution LiCl with constant stirring, after that the solution was diluted to mark with distilled water. After that the solutions of lower concentrations were prepared by dilution method. These solutions were used in NMR experiments (self-diffusion for ^{133}Cs, and ^{1}H nuclei, spectra on ^{133}Cs) and cryoscopy experiments. The total amount of samples was 5 and 17 for NMR and cryoscopy experiments respectively. In the table 1 the concentrations of the salts in the ternary systems are presented.

Table 1. Concentrations of the components in the ternary systems.

$MgCl_2 - CsCl - H_2O$		$MgCl_2 - LiCl - H_2O$		$LiCl - CsCl - H_2O$	
C($MgCl_2$)	2.38 M	C($MgCl_2$)	1.43 M	C(LiCl)	10 M
C(CsCl)	4.26 M	C(LiCl)	10.02 M	C(CsCl)	5 M

3.2 Cryoscopy experiment

Cryoscopy measurements were performed for all ternary systems on cryoscopic equipment presented in figure 4.

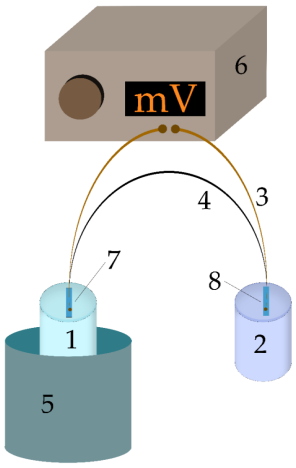

Figure 4. Cryoscopic setup scheme.

1. Dewar with a solution of the ternary system and a stirrer
2. Thermos with ice ($0°C$)
3. Copper wire
4. Constantan wire
5. Cryogenic storage dewar with liquid nitrogen
6. Digital microvoltmeter
7. Work junction
8. Cold (reference) junction

For cryoscopic measurement 25 ml of the studied solution were poured into dewar (1) and the work junction (7) of the thermocouple was placed inside the solution. Dewar (1) was slowly cooled with liquid nitrogen (5). Reference junction (8) was placed inside the thermos (2) with ice at constant temperature $0°C$. The voltage in the thermocouples changes due to the thermoelectric effect, at two ends of thermocouple there is different temperature, which creates potential difference. A temperature-dependent voltage (μV) was detected by digital microvoltmeter (6). At the moment of phase transition (liquid-solid) a jump in potential was observed. This value was compared with the voltage values on the calibration curve to establish the freezing temperature. Measurements were repeated for several times to determine the experimental error.

3.3 NMR experiment details

For systems $LiCl-CsCl-H_2O$, $MgCl_2-LiCl-H_2O$ and $MgCl_2-CsCl-H_2O$ the water molecules self-diffusion coefficients were measured (on ^1H nucleus) at room temperature $25°C$. Measurements for self-diffusion coefficients were done using Bruker 500 MHz Avance III spectrometer equipped with a 5 mm Bruker single-axis Diff 50 Z-diffusion probe. Diffusion coefficients (D) were obtained by Pulsed Field Gradient (PFG) NMR technique. For system $MgCl_2-CsCl-H_2O$ relaxation times were recorded for ^{133}Cs nucleus (since Mg nucleus is not sensitive enough for NMR method) at the temperature range from $25°C$ to freezing temperature with $5°C$ step. The relaxation times were measured using Bruker 500 MHz Avance III NMR Spectrometer. The longitudinal (spin lattice) T_1 relaxation time measurements were carried out using the inversion-recovery sequence (16 points per curve; monoexponential regression fitting with OLS of spectral line area). The amount of scans was 4 or 8, the experiment was repeated for the second set of solutions with concentrations within the margin of error. The probe temperature was maintained at $25°C$ (with accuracy $\pm$ $1°C$), with $5°C$ step for temperature dependence experiments.

To eliminate the inhomogeneity of the field in the sample, the spectrum in the system $LiCl-CsCl-H_2O$ for nuclei ^{133}Cs (resonant frequency 65.598 MHz) was obtained by the following method. Reference sample with known LiCl and CsCl concentrations was placed into spectrometer, the temperature was establishing for 10 minutes at $15°C$. The spectra were recorded on ^1H nuclei and the field uniformity was set. The spectra then were recorded on ^{133}Cs nuclei and one symmetrical peak was recorded. After that the studied solution was placed into spectrometer and the temperature was establishing for 10 minutes at $15°C$ as well. The spectra were recorded on ^{133}Cs nuclei. The sample was removed from the spectrometer, it was visually established that there was only the liquid phase in the ampoule. Then the reference sample was again placed into the spectrometer and spectra were recorded again on ^1H and ^{133}Cs nuclei, the magnetic field uniformity was confirmed. Shooting spectra were performed using 90-FID sequences and Fourier processing. A total of 64 scans were taken for a single spectrum.

3.4 X-ray crystallography and Powder diffraction

Single crystals were grown from concentrated solutions in desiccators over a sulfuric acid at $25°C$ in a thermostat. Periodically air was pumped out from desiccators to create a vacuum and more efficient dehydration environment. XRC analysis was performed on a single-crystal diffractometer Oxford Diffraction "Xcalibur". The sample was frozen

to 100K. Results of X-ray analysis were obtained using the program Olex2 (OLEX2: a complete structure solution, refinement and analysis program O. V. Dolomanov, L. J. Bourhis, R. J. Gildea, J. A. K. Howard and H. Puschmann) developed for the visualization and analysis of crystals. The structure was determined using the ShelXL program with the least squares method.

Samples for powder diffraction were dried in vacuum while heating and pounded into fine powder. Samples were radiographed to determine the phase composition with automatic diffractometer Bruker Phaser D2: radiation 1.5444 Å, tube operation mode $30kV/10mA$, position sensitive detector, reflection geometry, Bragg-Brentano focusing scheme, sample rotation speed of 20 revolutions per minute, diffraction angle interval $2\theta = 6 - 90^{\circ}$, $T = 25^{\circ}C$, the atmosphere is air. The sample was prepared by dry pressing the test mixture into a cuvette.

3.5 Calorimetry experiment

In this work, we used a conductive microcalorimeter of the Calvet type, equipped with two differential calorimetric cells. This device allows to record time-resolved difference in heat flow in the working cell and in the comparison cell. Two calorimetric cells are equipped with glasses of 35 mm diameter and a height of 80 mm. Each cell is equipped with thermocouples consisting of semiconductor thermoelectric elements. The calorimeter thermoblock consists of massive (20 kg) heat-leveling aluminum kernels with two symmetrically located calorimetric cells: working and reference. The gap between the thermoblock and the calorimeter jacket makes 20–25 mm. To average the temperature gradient of the thermal flow created around the fuser, the gap is filled up with foam. The calorimeter's shirt is separated from the environment by another layer of foam, to reduce the temperature effects from atmospheric air. The calorimeter is equipped with a mixing system. The figure 5 shows the calorimeter setup with the symmetric calorimetric cells.

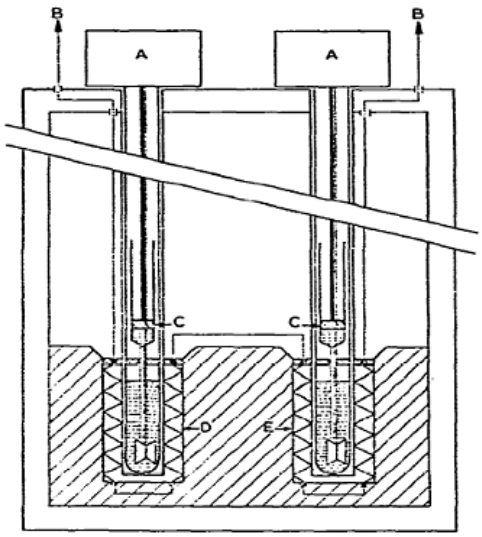

Figure 5. Calorimeter setup.

The calorimetric cell is an aluminum thin-walled glass with a diameter of 35 mm and a height of 80 mm (working volume of the cell is 50 ml). On the double-sided heater outer surface there is wound from a constantan wire with a diameter of 0.1 mm. The heater is laid in a special groove with a depth of 0.3 mm. Anticipatorily the surface of the latter was oxidized to avoid electrical closure of the heater and the cell. The contact of cells with the core is carried out by means of thermal converters. Calorimetric vessels are thin-walled titanium cups (0.5 mm), covered from the inside with a layer of teflon. The vessels are hermetically sealed with teflon lids, and the mixing of solution is achieved with a mechanical stirrer. The mixer helps to establish equilibrium faster in the calorimetric cup. The constancy of the core temperature is received by a water pumping through the calorimeter shirt and thermostatted with an U-10 ultra-thermostat at $25°C$ with an accuracy of $0.1°C$. The signal is registered by transmitting through an E-24 analog-digital converter manufactured by L-card to a personal computer. A calorimetric study was performed to determine the enthalpies of dissolution of double salts and dry mixtures of the components. 50 ml of distilled water was poured into the reference cell and into the working cell, and a sealed glass vial with a known amount of salt or mixture was placed inside the cell. After several hours when the baseline was established, the glass vial was broken, thus measuring the enthalpy of dissolution of the salts. The calorimeter was calibrated: the thermal effect of KCl dissolving was recorded and the calorimeter constant was calculated using literature data. The molar ratio of salt to water was kept at 1: 800, which corresponds to the infinitely diluted solution.

4 Results and discussion

Polythermal studies were conducted to clarify freezing temperatures of solutions, to find the composition corresponding to the eutectic point and to determine the number of structural zones of dominance in the ternary system with increasing salt concentrations. Generally, the liquid-solid phase transition was observed in these experiments. In the figure 6 (a,b and c) solubility diagrams of double solutions of cesium, lithium and magnesium chlorides are presented. On these phase diagrams, one can clearly see the difference between positively hydrated magnesium and lithium cations and negatively hydrated cesium cation. For magnesium and lithium chlorides solutions, there are various crystalline hydrates of different composition, low eutectic temperatures are very common for kosmotropic ions (m_{euth} (LiCl) = 7.8 mol/kg, $T_{fr} = -63^{\circ}C$, $m_{euth}(MgCl_2)$ = 2.75 mol/kg, $T_{fr} = -33^{\circ}C$), the position of the eutectic concentration is in the middle region of the concentration range. On the contrary, for a cesium chloride solution there are no crystalline hydrates, the freezing temperature of the eutectic composition is high ($T_{fr} = -23.2^{\circ}C$), the position of the eutectic concentration is shifted towards saturation concentration (m_{euth} (CsCl) = 8.07 mol/kg). In terms of percentage m_{euth} (LiCl) = 24 %, $m_{euth}(MgCl_2)$ = 22 %, m_{euth} (CsCl) = 59 %.

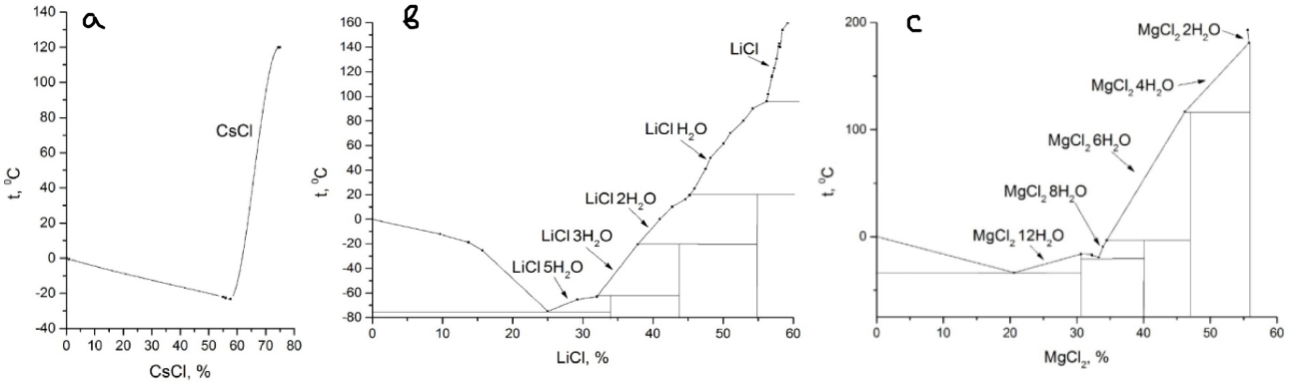

Figure 6. $CsCl-H_2O$, $LiCl-H_2O$ and $MgCl_2-H_2O$ phase diagrams [32].

On the solubility isotherm of the ternary system $MgCl_2-LiCl-H_2O$ [33, 34] there are three branches of crystallization, corresponding to the crystalline hydrates $MgCl_2 \cdot 6\,H_2O$ and $LiCl \cdot H_2O$ and double salt $MgCl_2 \cdot LiCl \cdot 7\,H_2O$. For polythermal measurements, a secant at the ratio Li / Mg = 7.03 was chosen, indicated in figure 7 with red line. It is seen that the secant ends at the crystallization branch of double salt.

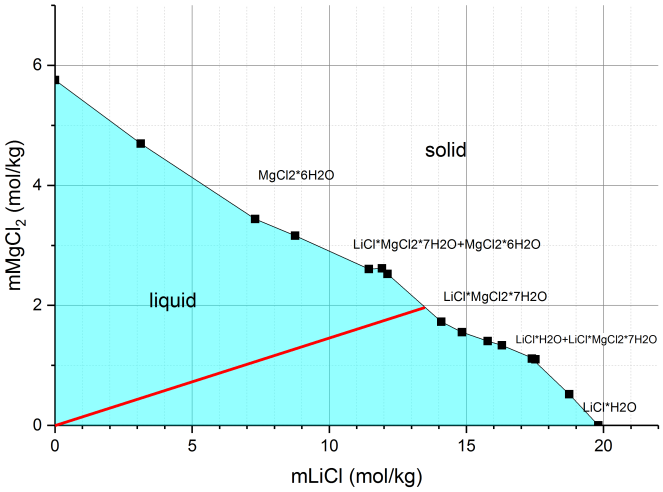

Figure 7. Solubility isotherm of the ternary $MgCl_2 - LiCl - H_2O$ system [33, 34].

Phenomenological model of the structure of concentrated electrolytes solutions states that in solutions of post-eutectic concentrations there is a change of solvent, and the constitution of the new dominant structure in the solution is similar to the structure of the solid phase crystallizing out with freezing. Polythermal studies of the freezing temperatures of solutions confirm the crystallization of only one compound after the eutectic point and the presence of only one crystallization domain for the selected ratio. If more than one compound crystallized on the section after the eutectic, a per-eutectic point would appear on the phase diagram. During the cryoscopic experiment, the glass transition region of the solution (m($MgCl_2$) = 1.4-0.98 mol/kg, m(LiCl) = 9.9-6.9 mol/kg) was detected, the eutectic temperature and concentration were determined by the extrapolation method. The presence of the glass transition region was expected, since even binary solutions of these chlorides freeze into a glassy mass upon sudden cooling, and the concentrations of such compositions are close to those obtained for the [35] ternary system. High affinity for water and the diagonal similarity of lithium and magnesium cations create conditions for competition for the water molecules in solution even before saturation. For a given concentration region, we should expect deviations in the water molecules mobility (diffusion rates) due to an increase in the solution viscosity. It can also be assumed that the double salt $LiCl \cdot MgCl_2 \cdot 7\,H_2O$ will be formed by the structure-induced conjugation mechanism, which can be confirmed by analyzing the structural features of its crystals by X-ray diffraction.

The Gibbs triangle (Fig. 8) consists of two phase diagrams of the binary systems $LiCl - H_2O$ and $MgCl_2 - H_2O$ [35], a freezing point of water, the solubility isotherm of the ternary system, taken from the literature data, and also the experimentally obtained sol-

ubility phase diagram over the selected concentration ratio of the ternary system, which is highlighted with black solid line. The concentration for Gibbs triangles is presented in terms of weight percentage. The eutectic point corresponds to $m(\mathrm{MgCl_2}) = 1.3$ mol/kg, $m(\mathrm{LiCl}) = 8.9$ mol/kg, in the terms of percentage it is $w(\mathrm{MgCl_2} = 8\%$ and $w(\mathrm{LiCl} = 25\%$. The freezing temperature is -128^0C.

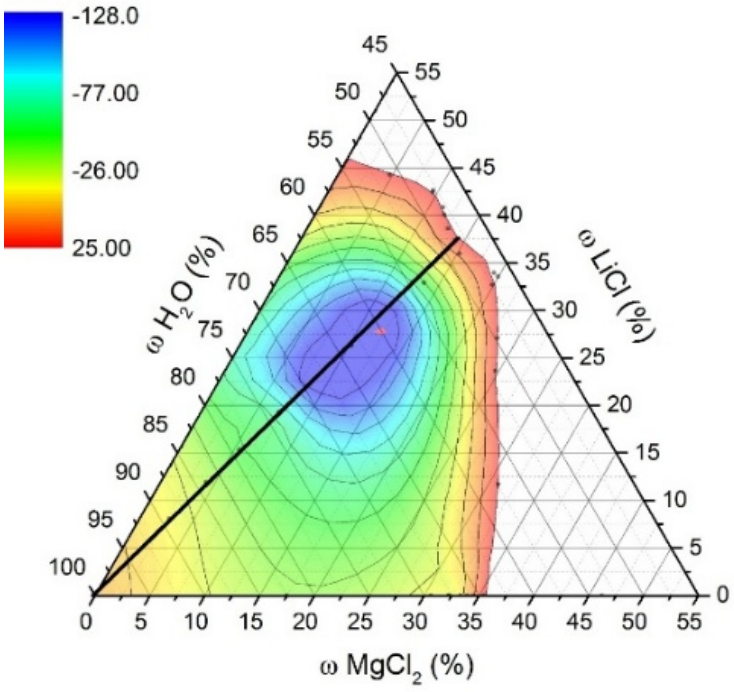

Figure 8. Gibbs triangle of the ternary $\mathrm{MgCl_2}-\mathrm{LiCl}-\mathrm{H_2O}$ system, black line represents investigated concentration secant.

In the ternary system $\mathrm{MgCl_2}-\mathrm{CsCl}-\mathrm{H_2O}$ on the solubility isotherm [33, 36] there are also three branches of crystallization. As can be seen in figure 9, magnesium chloride hexahydrate, anhydrous cesium chloride and the double salt $\mathrm{MgCl_2 \cdot CsCl \cdot 6\,H_2O}$ crystallize from this ternary solution. On the isotherm, a secant (red line) was chosen, which ends with the crystallization branch of the double salt. The Gibbs triangle of the ternary system (Fig. 10) was composed of two phase diagrams $\mathrm{MgCl_2}-\mathrm{H_2O}$, $\mathrm{CsCl}-\mathrm{H_2O}$ [35], the ternary solubility isotherm [33], taken from literature data, experimental freezing temperature data, and freezing point water. The black line corresponds to the investigated concentrations.

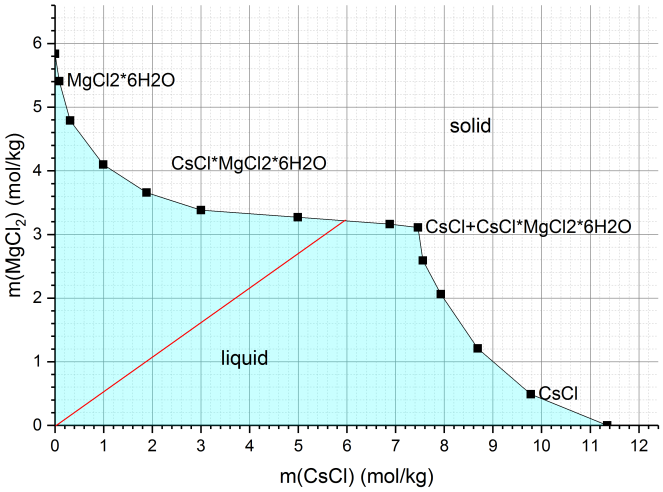

Figure 9. Solubility isotherm of the ternary system $MgCl_2-CsCl-H_2O$ [33, 36].

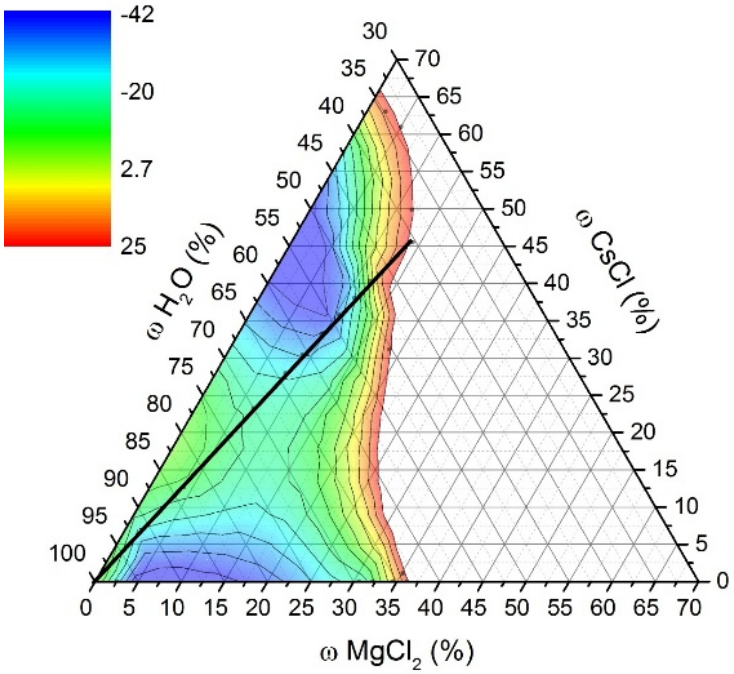

Figure 10. Gibbs Triangle for ternary system $MgCl_2-CsCl-H_2O$, black line represents investigated concentration secant.

Note the presence of one singular eutectic point (at a concentration of $m(\mathrm{CsCl}) = 3.95$ mol/kg, $m(\mathrm{MgCl_2}) = 2.03$ mol/kg, freezing temperature $-41°C$) and no glass transition domain. In terms of percantage the eutectic concentration is $w(\mathrm{MgCl_2} = 10.4\%$

and $w(\mathrm{CsCl} = 35.8\%$. In this regard, we can expect a smooth change in the structural-dynamic properties (such as relaxation times and the self-diffusion coefficient of water) as solution concentrates. Magnesium and cesium cations, which are different in the hydration way, also have very different sizes. Therefore, it can be assumed that a double salt is formed by the mechanism of structurally induced implantation.

For the ternary system $LiCl-CsCl-H_2O$ [37] freezing temperatures measurements were carried out on the secant with the ratio Li/Cs = 2/1, abutting on the crystallization branch of the $LiCl \cdot 3\,CsCl \cdot 4\,H_2O$ salt (Fig. 11).

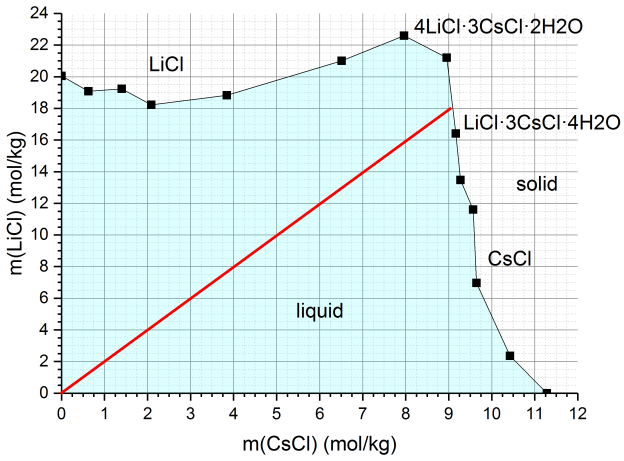

Figure 11. Solubility isotherm of the ternary system $LiCl-CsCl-H_2O$ [37].

An interesting feature of this system is the presence of a metastable region, after the concentration of 10 M by (Cl^-). Metastability manifested in the "premature" (before saturation) solid phase precipitation at room temperature in solutions with total chlorine concentrations from 14 to 22 mol/kg (> 10 mol/l) with $25°C$. On phase diagram this is reflected in the presence of a flat maximum in the specified posteutectic concentrations region (Fig. 12). It was not possible to determine the composition of the crystallizing out precipitate due to its instability and X-ray amorphism. To clarify the experimental results, freezing temperatures were also measured at a ratio of Li/Cs = 3/1, which corresponds to the crystallization branch of the compound $4\,LiCl \cdot 3\,CsCl \cdot 2\,H_2O$. The data confirmed the previously obtained results and the presence of metastability, which can be well seen from the Gibbs triangle (Fig. 13). The presence of a maximum on the phase diagram can be explained, for instance, by the fact that on the 2:1 secant there is a region of crystallization of the second double salt $4\,LiCl \cdot 3\,CsCl \cdot 2\,H_2O$, (that is, the crystallization fields of two

salts intersect). It can be assumed that the processes leading to formation of at least two different solid phases.

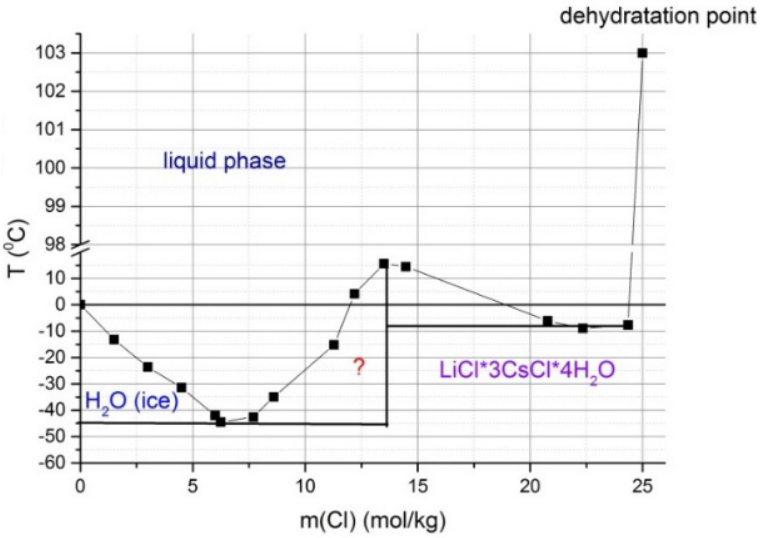

Figure 12. Phase diagram of the ternary system LiCl – CsCl – H_2O at ratio Li:Cs=2:1.

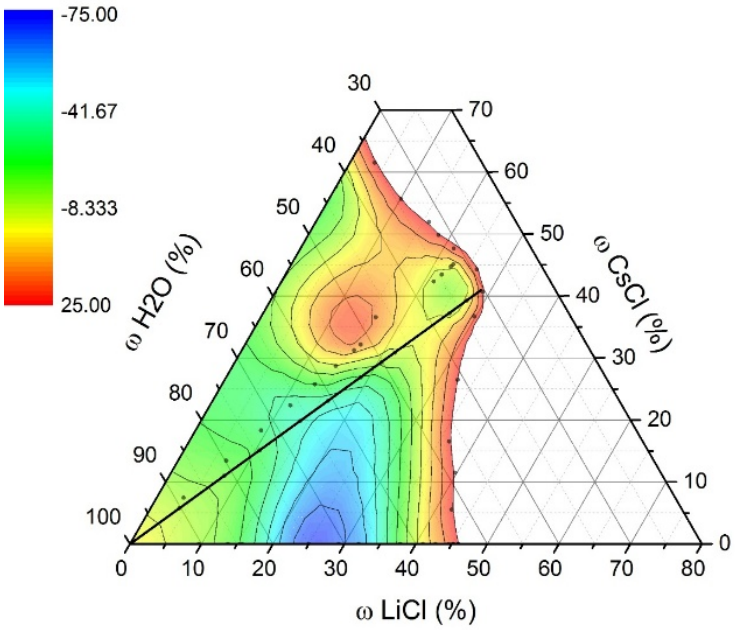

Figure 13. Gibbs Triangle for ternary System LiCl – CsCl – H_2O.

The eutectic concentrations are $m(\mathrm{CsCl}) = 2.4$ mol/kg, $m(\mathrm{LiCl}) = 4.8$ mol/kg, in the

terms of percentage it is $w(\mathrm{CsCl} = 22.4\%$ and $w(\mathrm{LiCl} = 11.2\%$. The freezing temperature is -42^0C.

4.1 X-Ray

As it is known, the method of X-ray analysis allows to obtain complete information on the structure of a crystal unit cell: distances between atoms, symmetry types, angles, and so on. Composition and structure of double salt and simple binary salts will help with further interpretation of experimental results.

4.1.1 $MgCl_2 \cdot CsCl \cdot 6\,H_2O$

Figure 14 shows the unit cell of the double salt $MgCl_2 \cdot CsCl \cdot 6\,H_2O$ and its main crystallographic parameters are given in the table 2. It can be seen that Mg is surrounded by six water molecules, and forms a regular octahedron (Fig. 15) with O-Mg-O angles as indicated in table 3. The distance between the nearest Mg atoms is 6.7258 Å. The distance between O and Mg atoms is 2.071 Å.

Table 2. X-ray diffraction parameters of double salt $MgCl_2 \cdot CsCl \cdot 6\,H_2O$.

Formula sum	Cl3 H12 Cs Mg O6
Formula weight	371.67 g/mol
Crystal system	monoclinic
Space-group	C 1 2/c 1 (15)
Cell parameters	a=9.4134(3) Å b=9.6425(3) Å c=13.4708(3) Å β=90.280(3)
Cell ratio	a/b=0.9762 b/c=0.7158 c/a=1.4310
Cell volume	1222.71(6) Å3
Z	4
Calc. density	2.01891 g/cm3
RAll	0.0322
Pearson code	mC100
Formula type	NO2P4Q6R12
Wyckoff sequence	f12e

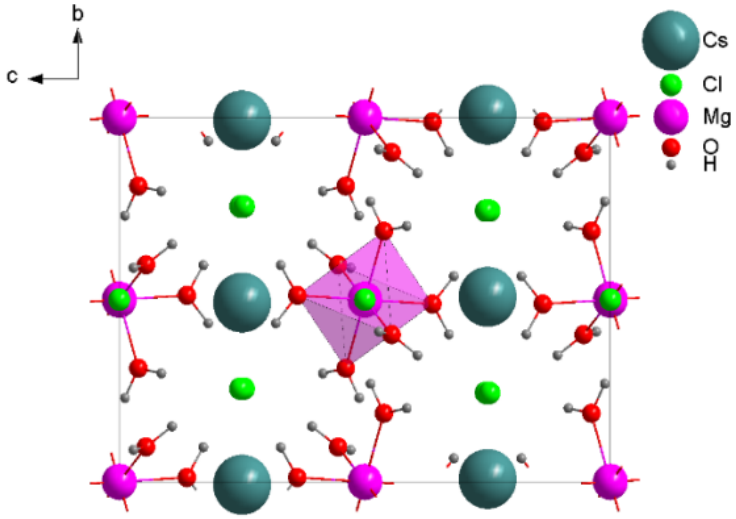

Figure 14. Unit cell of $MgCl_2 \cdot CsCl \cdot 6\,H_2O$ double salt, bc projection.

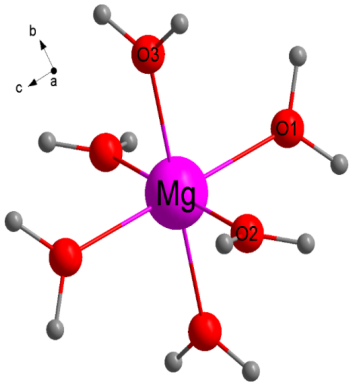

Figure 15. Octahedral environment of magnesium.

Table 3. The angles of the octahedron Mg.

Atom 1	Atom 2	Atom 3	Angle 2-1-3, deg
Mg	O3	O1	90.657
	O2	O3	91.074
	O1	O2	90.626

Magnesium octahedra are isolated from each other, as seen in the figure 16, they line up,

interspersed with rows of cesium rectangular prism, which are surrounded by chlorine atoms. It should be noted that cesium polyhedra have two common chlorine atoms with any neighboring cesium polyhedron, together they form an extended layered structure. The distance between the nearest Cs atoms are 6.7275 Å, and the distances Cs-Cl are 3.3686 Å.

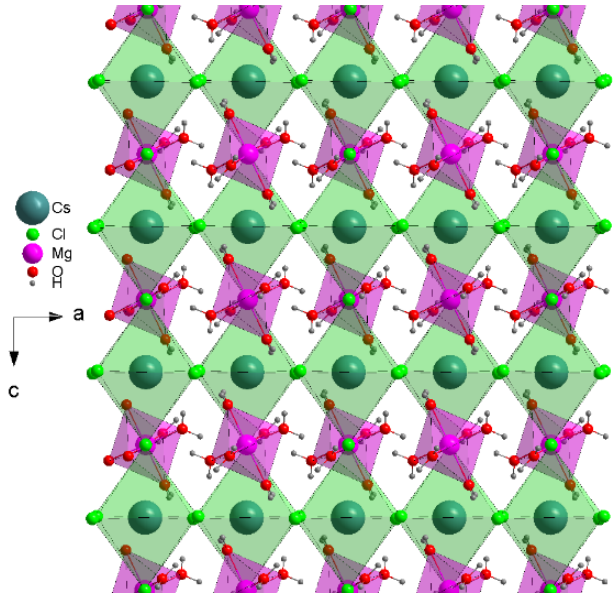

Figure 16. Double salt $MgCl_2 \cdot CsCl \cdot 6\,H_2O$ structure, ac projection.

4.1.2 $MgCl_2 \cdot LiCl \cdot 7\,H_2O$

Figure 17 shows the unit cell of the double salt $MgCl_2 \cdot LiCl \cdot 7\,H_2O$, and the table 4 shows the main crystallographic parameters. In this structure, Mg is also surrounded by 6 water molecules and forms a regular octahedron.

Table 4. X-ray diffraction parameters of double salt $MgCl_2 \cdot LiCl \cdot 7\,H_2O$.

Formula sum	Cl3 H12 Cs Mg O6
Formula weight	371.67 g/mol
Crystal system	monoclinic
Space-group	C 1 2/c 1 (15)
Cell parameters	a=9.4134(3) Å b=9.6425(3) Å c=13.4708(3) Å β=90.280(3)
Cell ratio	a/b=0.9762 b/c=0.7158 c/a=1.4310
Cell volume	1222.71(6) Å3
Z	4
Calc. density	2.01891 g/cm3
RAll	0.0322
Pearson code	mC100
Formula type	NO2P4Q6R12
Wyckoff sequence	f12e

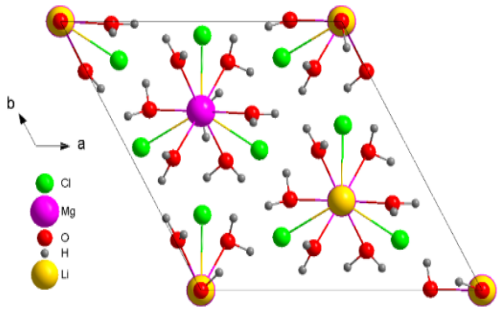

Figure 17. Unit cell of $MgCl_2 \cdot LiCl \cdot 7\,H_2O$ double salt, ba projection.

Magnesium octahedra are isolated from each other in this structure as well. The distance between the two nearest Mg atoms is 6.618 Å, which is 0.1 Å less than in the double salt $MgCl_2 \cdot CsCl \cdot 6\,H_2O$. The distances between the O atoms and the Mg atoms are 2.0630 Å, this value is slightly less than in $MgCl_2 \cdot CsCl \cdot 6\,H_2O$ double salt. In turn, Li surrounds itself with three Cl atoms and one water molecule, forms a tetrahedron (Fig. 18) with the angles indicated in the table 5.

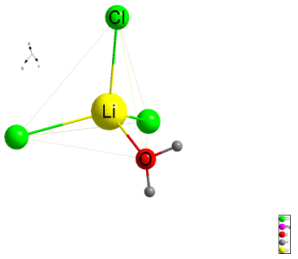

Figure 18. The tetrahedral environment of lithium.

Table 5. Angles in Li tetrahedron.

Atom 1	Atom 2	Atom 3	Angle 2-1-3, deg
Li	C1	O	109.27
	C1	C1	109.67

Lithium tetrahedra are also isolated from each other. The smallest distance between Li atoms is 6.6819 Å. The distances between Li-Cl and Li-O atoms are 2.3806 and 1.9075 Å, respectively. The Mg octahedra and Li tetrahedra create extended rows with alternating layers, however, polyhedra do not touch each other and do not form joint bonds, as shown in the figure 19.

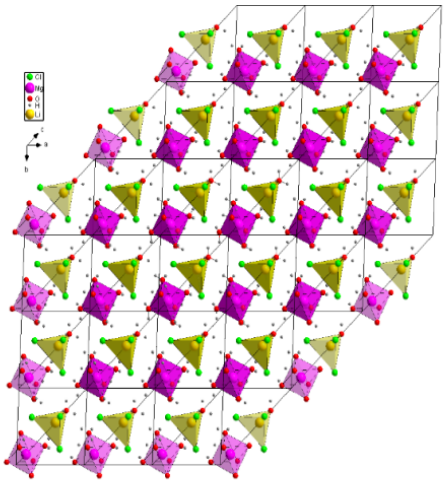

Figure 19. Structure of the $MgCl_2 \cdot LiCl \cdot 7\,H_2O$ double salt.

4.1.3 $LiCl \cdot 3\,CsCl \cdot 4\,H_2O$

The table 6 presents the main X-ray structural $LiCl \cdot 3\,CsCl \cdot 4\,H_2O$ double salt parameters. The main results and conclusions on the structure of the double salt and the interaction of individual cations were made earlier [38]. Here are the main parameters for comparison and brief conclusions based on previous studies. Figure 20 shows double salt structure.

Table 6. X-ray diffraction parameters of double salt $LiCl \cdot 3\,CsCl \cdot 4\,H_2O$.

Formula sum	Cl4 Cs3 Li O4
Formula weight	611.47 g/mol
Crystal system	tetragonal
Space-group	P 4/n m m (129)
Cell parameters	a=8.5827(4) Å c=9.9799(7) Å
Cell ratio	a/b=1.0000 b/c=0.8600 c/a=1.1628
Cell volume	735.15(9) Å3
Z	2
Calc. density	2.76219 g/cm3
RAll	0.0301
Pearson code	tP32
Formula type	NO3P4Q8
Wyckoff sequence	kic2ba

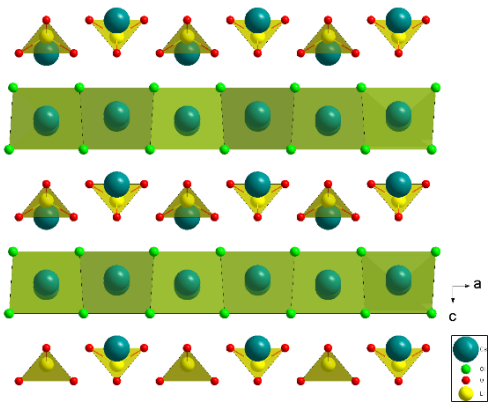

Figure 20. Structure of $LiCl \cdot 3\,CsCl \cdot 4\,H_2O$ double salt, projection ac.

The results of X-ray structural analysis showed that lithium is surrounded with 4 water molecules, forming a distorted tetrahedron. Chlorine, in its turn, surrounds Cs atoms, forming rectangular prisms. Prisms and tetrahedrons replace each other in layers. The tetrahedron (Fig. 21), where lithium is surrounded by 4 water molecules, is distorted with angles of 105,462° and 117,828°. This distortion can be explained by the presence of cesium ions, which are positively charged ions and, consequently, they must enter into electrostatic interactions with hydrogen atoms located near oxygen.

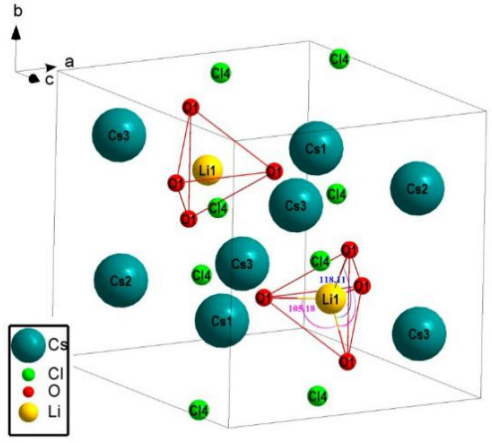

Figure 21. Distorted tetrahedral lithium in the unit cell of the $LiCl \cdot 3\,CsCl \cdot 4\,H_2O$ double salt.

The minimum Li-O distance is 1.9503 Å, the minimum distance Li-Li is 6.0689 Å. The angles are presented in table. 7, and the corresponding atom numbers are indicated in the figure 22.

Table 7. Li tetrahedron.

Atom 1	Atom 2	Atom 3	Angle 2-1-3, deg
Li	O1	O2	105.462
	O1	O3	105.462
	O1	O4	117.828
	O2	O3	117.828
	O2	O4	105.462
	O3	O4	105.462

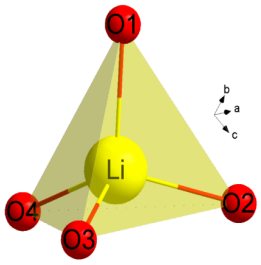

Figure 22. The tetrahedral environment of lithium.

The Cs polyhedra are also of a great interest, they are tightly bound to each other with help of 4 common Cl atoms (3.5612 Å), forming continuous layers. Moreover, it is interesting that one of the Cs atoms includes in its environment 4 water molecules located at a distance of 3.2906 Å. Despite the fact that CsCl itself does not form crystalline hydrates, in this double salt there is a bond between Cs and O, which certainly must influence the structural and dynamic properties of the concentrated solution. The distances Cs_2 – Cs_3 are 4.2998 Å, Cs_2 – Cs_1 are 5.8717 Å, and Cs_1 – Cs_3 4.2773 Å. This is significantly (on average, by 1.5 Å) a smaller distance than in the structure of the double salt $MgCl_2 \cdot CsCl \cdot 6\,H_2O$, which indicates a more dense distribution of cesium in a single isolated structure Cs_xCl_y.

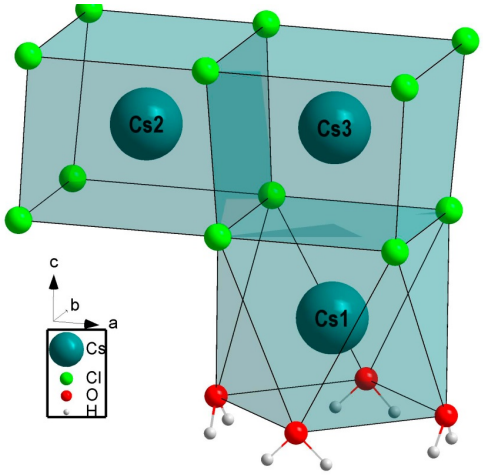

Figure 23. Cesium polyhedra.

4.1.4 $4\,LiCl \cdot 3\,CsCl \cdot 2\,H_2O$

The table 8 shows the main crystallographic parameters of $4\,LiCl \cdot 3\,CsCl \cdot 2\,H_2O$ double salt. A new salt $4\,LiCl \cdot CsCl \cdot 2\,H_2O$, unknown earlier was obtained from a concentrated solution at a ratio of Li/Cs = 3:1. The structure and the main crystallographic parameters was deciphered and identified. Key cell parameters and results are presented in the paper [38]. Here one can compare its parameters and structure with previously described double salts.

Table 8. X-ray diffraction parameters of double salt $4\,LiCl \cdot 3\,CsCl \cdot 2\,H_2O$.

Formula sum	Cl7 Cs3 H4 Li4 O2
Formula weight	710.67 g/mol
Crystal system	monoclinic
Space-group	C 1 2/c 1 (15)
Cell parameters	a=13.0159(4) Å b=14.9326(4) Å c=9.2384(2) Å β=105.750(3)^0
Cell ratio	a/b=0.8716 b/c=1.6164 c/a=0.7098
Cell volume	1728.17(8) Å3
Z	4
Calc. density	2.73127 g/cm3
RAll	0.0283
Pearson code	mC80
Formula type	N2O3P4Q4R7
Wyckoff sequence	f9e2

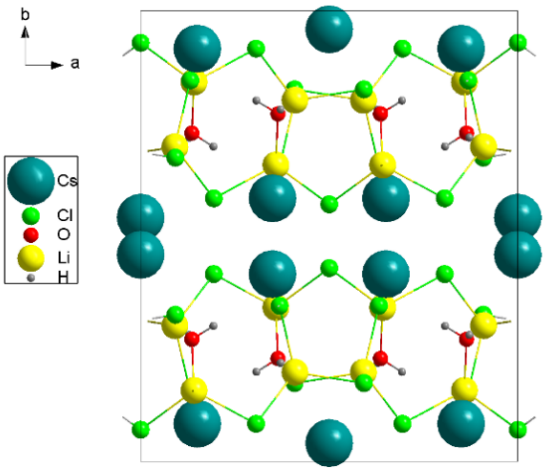

Figure 24. A unit cell of the double salt $4\,LiCl \cdot 3\,CsCl \cdot 2\,H_2O$, projection ab.

This structure is a complex system consisting of related Li tetrahedron with embedded Cs atoms as shown in the figure 24. According to the X-ray diffraction experimental results, Li forms tetrahedrons of two types. The first type of tetrahedra includes only Cl atoms, the second type includes Cl atoms and water molecules. Tetrahedra are bound in different ways in each case. Tetrahedra of the first type are bound together by one chlorine atom, the second type is bound by two chlorines atoms and the first with the second types are linked by only one chlorine atom as shown in figure 25.

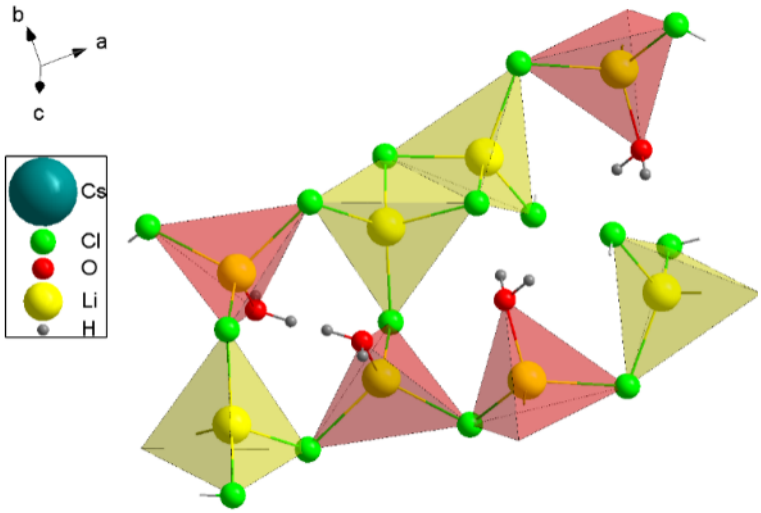

Figure 25. Lithium tetrahedron system.

Distances Li – Cl are approximately constant $2.4 - -2.3$ Å, the distance Li-O equals

1.9277 Å, which slightly diverges from the distances between the corresponding atoms obtained in other double salts. The distance Li-Li is approximately 3.7 Å, in this double salt cations distribution is significantly denser (on ~3 Å) than in the structure of $LiCl \cdot 3\,CsCl \cdot 4\,H_2O$ and $MgCl_2 \cdot LiCl \cdot 7\,H_2O$ double salts.

The arrangements of Cs and Cl atoms in this structure are irregular, Cs does not create the regular symmetric polyhedron. The distances to the nearest Cl atoms are within 3.4 Å, and although these are shorter distances than in the structures $LiCl \cdot 3\,CsCl \cdot 4\,H_2O$ or $MgCl_2 \cdot CsCl \cdot 6\,H_2O$, there are no regular prisms around Cs as shown in figure 26.

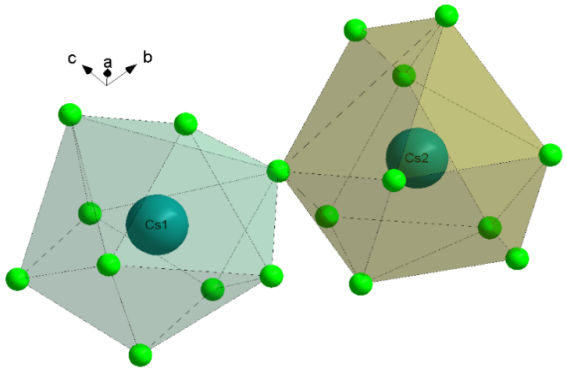

Figure 26. The asymmetric environment of cesium.

Comparison of crystal structures of double salts with features of the binary salts of cesium chloride CsCl, magnesium $MgCl_2 \cdot xH_2O$ and lithium $LiCl \cdot xH_2O$ crystallohydrates gives a better complete picture on the ions interaction. Figure 27 shows the environment of lithium ion in the crystal lattice of the lithium chloride monohydrate $LiCl \cdot H_2O$ [39]. It can be seen that lithium forms a regular octahedron with $4\,Cl^-$ ions and two water molecules. The distances between the centers of the ions are given in table 9.

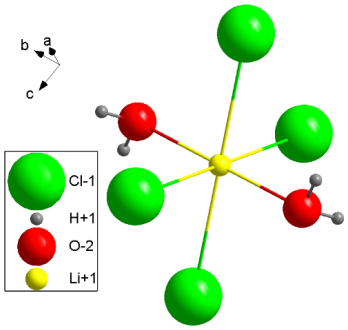

Figure 27. Lithium environment in crystal structure of $LiCl \cdot H_2O$.

Table 9. The distance Li-closest atoms.

Atom1	Atom2	Distance, Å
Li1	O	2.0363
	Cl	2.6302
	Li2	3.0763

The main and the greatest property in comparison with the double salts is in the different symmetry of the nearest surrounding of Li ions. In $LiCl \cdot H_2O$ structure and other crystallohydrates, as it will be shown further, Li forms an octahedral environment. They line up in long non-insulated layers, with distances between the polyhedra centers twice times smaller than for double salts. Exception here makes the crystal structure of the double salt $4\,LiCl \cdot 3\,CsCl \cdot 2\,H_2O$, which is also characterized by small distances between Li – Li, indicating a dense cations distribution.

Crystal structure of lithium chloride dihydrate $LiCl \cdot 2\,H_2O$ [40] is shown in figure 28. Here the lithium environment is also octahedral, it includes two Cl atoms and 4 water molecules. The distances between the centers of atoms are shown in table 10, they are not much different from the previous structure of $LiCl \cdot H_2O$. Interesting moment is the asymmetric arrangement of the chlorine atoms in octahedron. The first atom is located in the axial position, and another atom is in the equatorial position. Lithium octahedra are joined together alternately by two water molecules or by one water molecule and chlorine atom. They also form long chains, which are not located in one plane and do not form flat layers.

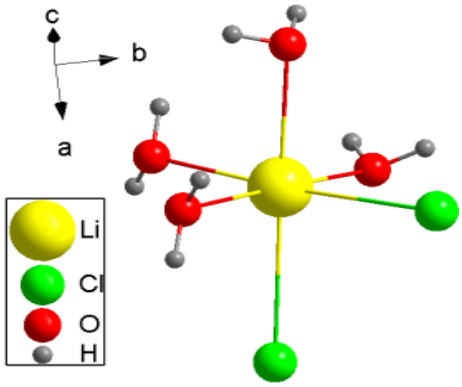

Figure 28. The environment lithium in the crystal structure of crystalline hydrate $LiCl \cdot 2\,H_2O$.

Table 10. Distances between Li and its nearest environment.

Atom1	Atom2	Distance, Å
Li1	O	2.0835
	Cl	2.6643
	Li2	3.0977

The trihydrate lithium chloride $LiCl \cdot 3\,H_2O$ [40] is shown in figure 29. Lithium is surrounded by a regular octahedron comprising 2 chlorine atoms in the axial position and 4 water molecules in the equatorial position. The distances between atoms are presented in table 11. The main feature of this structure it is that lithium octahedra have 2 common water molecules, despite the overall increase of water molecules amount, the cations distribution becomes denser and the atoms are forced closer to each other. Lithium polyhedra are lining up in extended layers.

Table 11. The distance Li-closest surrounding.

Atom1	Atom2	Distance, Å
Li1	O	2.0599
	Cl	2.6989
	Li2	2.8019

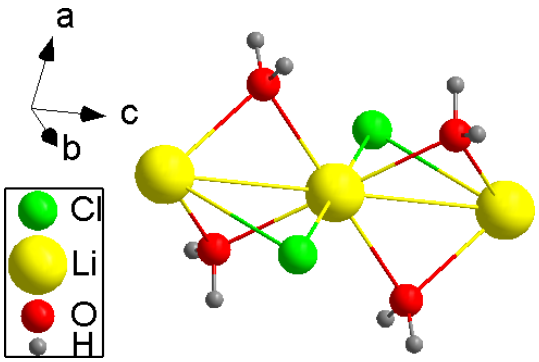

Figure 29. The environment lithium in the crystal structure of crystalline hydrate $LiCl \cdot 3\,H_2O$.

Figure 30 shows the environment of lithium in a crystalline structure of lithium chloride pentahydrate $LiCl \cdot 5\,H_2O$ [40]. In this salt the number of water molecules is the largest and lithium can build a distorted octahedron around itself, consisting exclusively of water molecules. Chlorine atoms are also coordinated by 4 water molecules in a form of a tetrahedron. The distances between atoms are presented in the table 12, they also do not differ much from the previous crystallohydrates examples. For this structure, a characteristic feature is the distortion of the lithium octahedron and the connection of the octahedrons by two water molecules to each other. In the pentahydrate of lithium chloride the smooth extended layers are formed.

Table 12. The distance Li-closest surrounding.

Atom1	Atom2	Distance, Å
Li1	O_{axial}	2.1898
	$O_{equatorial}$	2.1053
	Cl	4.5654
	Li2	3.1094

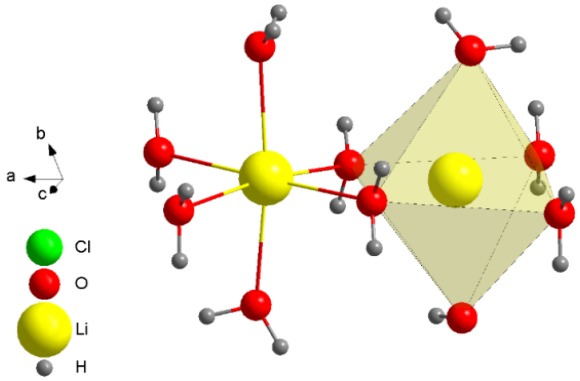

Figure 30. The environment lithium in the crystal structure of crystalline hydrate $LiCl \cdot 5\,H_2O$.

The comparison of the double salts with simple binary crystalline hydrates of lithium chlorides gives the notion that, first of all, lithium coordination in these structures is octahedral – whereas for double salts there is a tetrahedral lithium environment. It is logical that the implementation of additional salts will decrease the average number of water molecules per ion, and for complete hydration the amount of water molecules may not be enough. It is interesting to consider Li-Li distances in terms of cation density distributions. For double salts with lithium, these distances are 6,6819 Å for $MgCl_2 \cdot LiCl \cdot 7\,H_2O$, 6,0689 Å for $LiCl \cdot 3\,CsCl \cdot 4\,H_2O$, 3.7 Å for $4\,LiCl \cdot 3\,CsCl \cdot 2\,H_2O$, whereas for crystallohydrates of lithium chloride, the Li-Li distances fluctuate in the range of 3 Å. Then, we can conclude that in double salts of $LiCl \cdot 3\,CsCl \cdot 4\,H_2O$, $MgCl_2 \cdot LiCl \cdot 7\,H_2O$ lithium cations experience denser distribution, lithium is forced to be isolated and to increase the distance between the charged cations. The same does not appeal for structure of $4\,LiCl \cdot 3\,CsCl \cdot 2\,H_2O$, where Cs is located irregularly, lithium tetrahedra are located close to each other producing long layers, indicating the changes of the nearest Li environment. Which can occur due to increase in the number of Li cations in the unit-cell formula as well as presence of CsCl.

The figure 31 represents characteristic environment of magnesium atom in the crystal lattice of different $MgCl_2 \cdot xH_2O$. The exceptions here are crystallohydrates of $MgCl_2 \cdot 4\,H_2O$ [41] and $MgCl_2 \cdot 2\,H_2O$ [42]. For $MgCl_2 \cdot 4\,H_2O$ the structure is presented on figure 32, here magnesium environment includes two chlorine atoms. Octahedral environment of magnesium in structure $MgCl_2 \cdot 2\,H_2O$ is shown in figure 33, here magnesium is surrounded by 4 chlorine atoms, and forms extended layers where magnesium octahedra are connected by 2 chlorine atoms. It should also be noted that the isolated Mg octahedra are formed in the crystalline hydrates: $MgCl_2 \cdot 4\,H_2O$, $MgCl_2 \cdot 6\,H_2O$, $MgCl_2 \cdot 8\,H_2O$

and $MgCl_2 \cdot 12\,H_2O$. To sum up in each crystalline hydrate except $MgCl_2 \cdot 2\,H_2O$. This is clearly noticeable by distances Mg-Mg described in the paper ([41]).

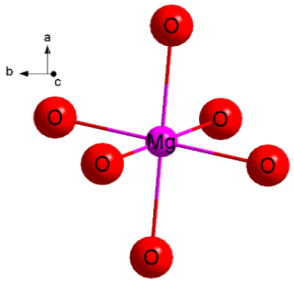

Figure 31. A typical environment of magnesium in the structures of crystalline hydrates.

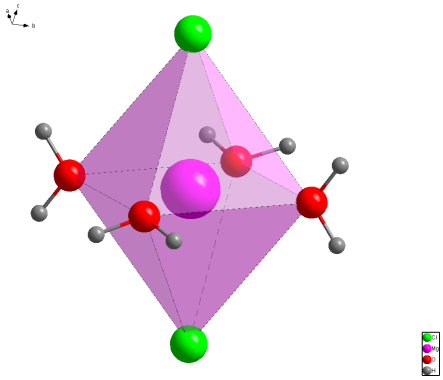

Figure 32. The octahedral environment of magnesium in the structure of crystalline hydrate $MgCl_2 \cdot 4\,H_2O$.

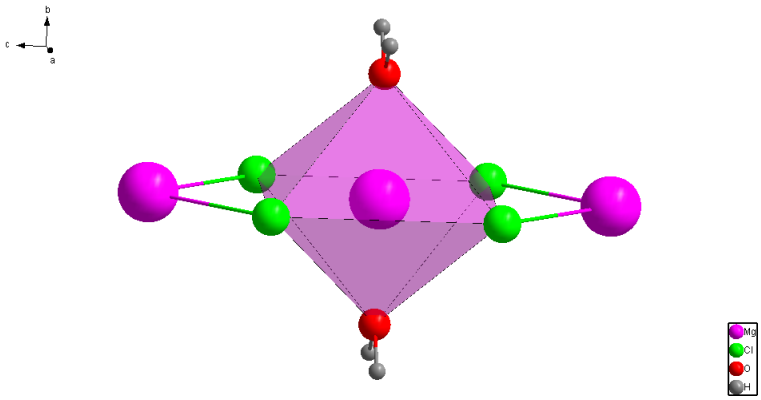

Figure 33. The octahedral environment of magnesium in the structure of crystalline hydrate $MgCl_2 \cdot 2\,H_2O$.

Table 13 presents the distances between Mg-Mg atoms. It is noticeable that the distance of Mg-O does not undergo significant changes in all crystal structures.

Table 13. The distance between Mg and it's closest environment in the crystalline hydrates.

dMg-A2	$MgCl_2 \cdot 12\,H_2O$	$MgCl_2 \cdot 8\,H_2O$	$MgCl_2 \cdot 6\,H_2O$	$MgCl_2 \cdot 4\,H_2O$	$MgCl_2 \cdot 2\,H_2O$
Mg-Mg	7.3496	6.7482	6.1000	5.5607	3.6507
Mg-O	2.06	2.0349	2.0399	2.0523	2.0079
Mg-Cl	4.8	4.5	4.0569	2.5515	2.5

Figure 34 shows the crystal structure of the CsCl salt [43]. In this structure Cs has a rectangular prism environment, which consists of 8 chlorine atoms, each polyhedron teaming up with a neighbor with 4 chlorine atoms. Distances are represented in the table 14.

Table 14. The distance between the nearest environment of Cs.

Atom1	Atom2	Distance, Å
Cs1	Cs2	3.5637
	Cl	4.1150

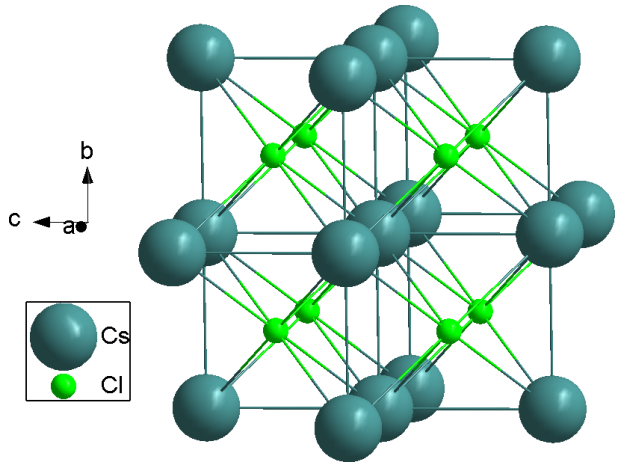

Figure 34. Crystal structure of salt CsCl.

Based on comparisons of the crystal structures of the $LiCl \cdot xH_2O$, $MgCl_2 \cdot xH_2O$ and CsCl simple binary salts and double salts it is possible to draw the following conclusions.

- In the crystal structure $MgCl_2 \cdot CsCl \cdot 6\,H_2O$ there is a combination of two sub-structures: $MgCl_2 \cdot 6\,H_2O$ and CsCl. The Mg environment does not change, the polyhedra remain isolated, the distance between Mg increases slightly by 0.5 Å in comparison to the crystalline hydrates. In the Cs polyhedra the center atoms are driven apart by significant ~3 Å forming isolated polyhedra. Thus, we can talk about the combination broken sub-structure of anhydrous cesium chloride and sub-structures magnesium chloride hexahydrate $MgCl_2 \cdot 6\,H_2O$.

- In crystal structure of $MgCl_2 \cdot LiCl \cdot 7\,H_2O$ magnesium environment does not differ a lot from those of the binary crystallohydrates. Whereas the Li environment changes significantly. Li polyhedra symmetry changes from octahedral to tetrahedral, such tetrahedral symmetry is characteristic for lithium ion in the solution. The distance between the centers of tetrahedra are increased up to ~3 Å in comparison with binary salts. The nearest Li environment is preserved with characteristic distances Li-Cl, Li-O. In this case, we observe the combination of the chloride hexahydrate magnesium $MgCl_2 \cdot 6\,H_2O$ sub-structure and fragmented lithium with its closest environment.

- In crystal structure of $LiCl \cdot 3\,CsCl \cdot 4\,H_2O$ the nearest lithium environment is changed as well. Symmetry changes from octahedral to tetrahedral, in the Li environment there are 4 water molecules, the distances Li-O are the same as in crystallohydrates, while Li-Li distances increase by ~3 Å. In this case Cs atoms are coordinated by chlorine atoms, however besides these, there are 4 water molecules, and forms a spatially united structures. Mechanism of formation of this salt is structurally forced introduction of lithium fragments and its environments in the sub-structure of anhydrous cesium chloride CsCl.

- And finally in the crystal structure $4\,LiCl \cdot 3\,CsCl \cdot 2\,H_2O$ there are significant changes in the Cs environment. Cesium does not form any symmetric polyhedra, despite the fact that the nearest distance to Cl are somewhat closer than in the simple structure of CsCl. Naturally there is a slight increase in the distances between Cs atoms. The Cs polyhedra are isolated, in contrast to the Li tetrahedra are united through shared chlorine atoms in the extended ribbon structure. It is possible to conclude that this double salt is formed by the introduction of cesium fragments in the sub-structure of lithium and its surroundings.

Thus, it is possible to identify the main patterns of double salts formation mechanisms.

1. The sub-structure of $MgCl_2 \cdot 6\,H_2O$ is robust, Mg with enviable consistently sur-

rounds itself with 6 water molecules, forming isolated octahedrons. Such regularities are characteristic for double salts and water binary crystallohydrates.

2. The CsCl substructure undergoes changes in cases of all double salts, sometimes even collapses completely into fragments.

3. The Li environment undergoes the biggest changes in symmetry. The differences between double salts and crystallohydrates appear due to the presence of extraneous sub-structures. Li is forced to vary its environment to form a joint compounds, create a bonded network, adjust and integrate into the environment.

4.2 Powder diffraction

X-ray phase analysis was carried out in parallel with the calorimetric experiment for the same double salts. This experiment was done because the thermal effects obtained from calorimetric measurements are extremely sensitive to impurities and excess of water. It was necessary to make sure that the samples contain only one pure phase with no impurities. Theoretical calculation of X-ray spectra (diffractograms) are produced using the program Diamond from the data of the XRC analysis. Comparison of the calculated and experimental diagrams gives a good match, it confirms the purity of the samples obtained for calorimetric experiments. The calculated and experimentally obtained diffraction pattern of the $MgCl_2 \cdot CsCl \cdot 6\,H_2O$ crystal structure is presented in figure 35. The red lines correspond to the calculated diffractograms, black are for experimental.

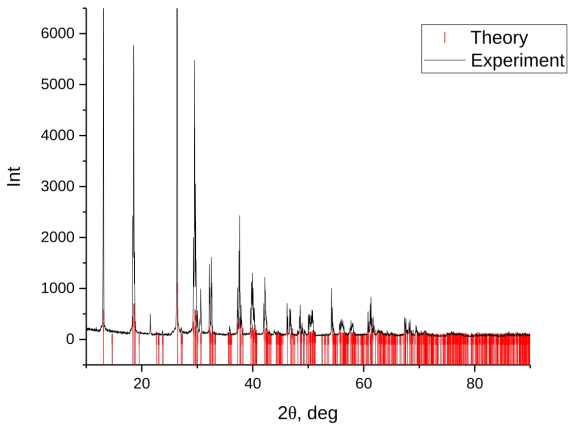

Figure 35. Comparison of calculated and experimental diffraction patterns of the double salt $MgCl_2 \cdot CsCl \cdot 6\,H_2O$.

The calculated and experimentally obtained diffraction pattern of the $MgCl_2 \cdot LiCl \cdot 7\,H_2O$

crystal structures are shown in the figure 36. The red lines correspond to the calculated diffractograms, black are for experimental.

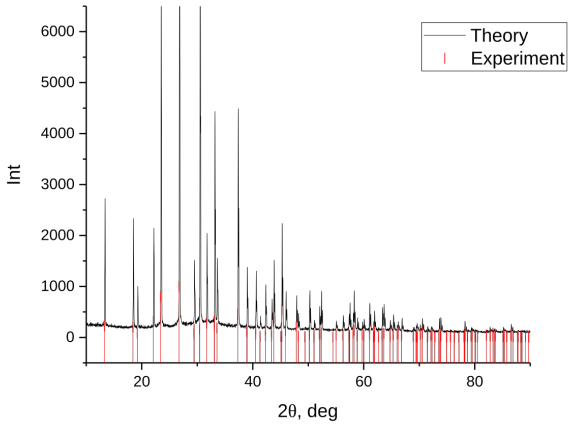

Figure 36. Comparison of the calculated and experimental diffraction patterns of the double salt $MgCl_2 \cdot LiCl \cdot 7\,H_2O$.

Comparative analysis of the calculated and theoretical diffractograms gives reasons to believe that in calorimetric studies there pure samples of the corresponding double salts were used.

4.3 Calorimetric measurements

Calorimetric measurements of the dissolution enthalpy of salts mixture and double salts were performed to determine the standard formation enthalpy of double salts. Table 15 represents the results of several measurements of the thermal effects of double salt $MgCl_2 \cdot CsCl \cdot 6\,H_2O$ dissolution. Where ν is mole, S is area under curve, Q is recalculated thermal effect

Table 15. Results of measurements of thermal effects of dissolution.

#	m, g	ν, mol	S, mVs	Q, kJ	H, kJ/mol	Error
1	0.0235	6.32213E-05	2.199555	8.207296	-129.8	-1.6
2	0.037	9.954E-05	3.359552	12.53564	-125.9	2.3
3	0.0302	8.12461E-05	2.764156	10.31402	-126.9	1.3
4	0.0392	0.000105459	3.678282	13.72493	-130.1	-1.9
					-128.2	**2.5**

Figure 37 traces three stages of calorimetric measurement. Stage 1 is establishment of the baseline, stage 2 is dissolution of the test substance (it requires to break the sealed ampoule with the substance inside), and stage 3 is establishment of the baseline. After that the mathematical processing followed, the integral of the area under the curve is indicated by the letter S, the thermal effect was calculated by the formula

$$S/k = Q \tag{4}$$

where k is the calorimeter constant, Q is the thermal effect. According to the known weight of the sample, the amount of moles of the substance was calculated, and the corresponding thermal effect was divided by the number of moles, the molar value (kJ/mol) was obtained. All measurements were carried out according to this method, so the final results are presented without intermediate processing.

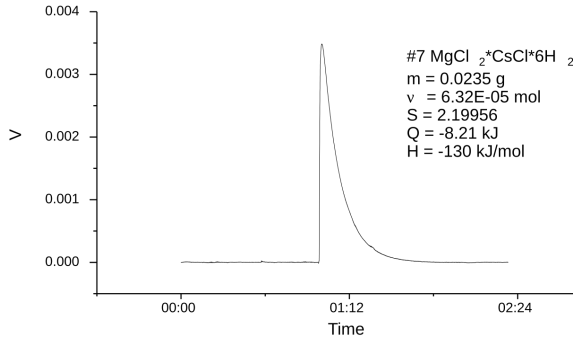

Figure 37. Calorimetry experiment curve, volts versus time dependence.

4.3.1 $MgCl_2 \cdot CsCl \cdot 6\,H_2O$

The dissolution enthalpy of the double salt $MgCl_2 \cdot CsCl \cdot 6\,H_2O$ is $-128kJ/mol$. For mixture of binary $MgCl_2 \cdot 6\,H_2O$ and CsCl the experimental value of the dissolution enthalpy is $-18kJ/mol$. Since the final states are the same (infinitely diluted solution), then according to Hess's law it is possible to draw a thermodynamic cycle, presented in figure 38.

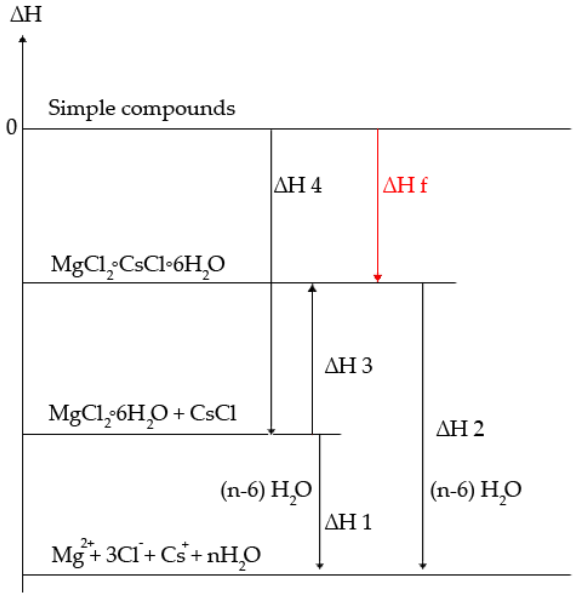

Figure 38. Thermochemical cycle of the system including Mg and Cs.

Here:

- ΔH_1^{∞} is dissolution enthalpy of salt mixture
- ΔH_2^{∞} is double salt dissolution enthalpy
- ΔH_3^0 is reaction [$MgCl_2 \cdot 6\,H_2O$] + [CsCl] = [$MgCl_2 \cdot CsCl \cdot 6\,H_2O$] enthalpy
- ΔH_4^0 is the sum of the standard enthalpies of formation [$MgCl_2 \cdot 6\,H_2O$] and [CsCl]
- ΔH_f^0 is the standard formation enthalpy of double salts

For the reaction of the a double salt formation from the constituent components

$$[\mathrm{MgCl_2 \cdot 6\,H_2O}] + [\mathrm{CsCl}] = [\mathrm{MgCl_2 \cdot CsCl \cdot 6\,H_2O}] \tag{5}$$

The thermal effect can be calculated by the following formula:

$$\Delta H_3^0 = \Delta H_1^0 - \Delta H_2^0 = -18 + 128 = 110 kJ/mol \tag{6}$$

From the literature data ([44], [45]) the ΔH_4^0 can be calculated:

$$\Delta H_4^0 = \Delta H_f^0(\mathrm{MgCl_2 \cdot 6\,H_2O}) + \Delta H_f^0(\mathrm{CsCl}) = -2498.852 + (-442.437) = -2941.29 kJ/mol \quad (7)$$

And the standard enthalpy of double salt formation can be calculated by the following formula:

$$\Delta H_f^0 = \Delta H_4^0 + \Delta H_3^0 = -2941 + 110 = -2831 kJ/mol \quad (8)$$

4.3.2 $\mathbf{MgCl_2 \cdot LiCl \cdot 7\,H_2O}$

As it is known, the Mg and Li crystallohydrates are extremely hygroscopic substances, and it is not surprising that their joint the compound is also a hygroscopic crystals, actively absorbing water from the air. For calorimetric measurements, the presence of excess water is critical and strongly affects the results. Calorimetric measurements were carried out with salts that were previously carefully weighed and dried in a vacuum with little heating until a constant mass was established. The difference in mass after drying and before drying is equal to the mass of the removed water. In total 9 measurements were made and a polynomial describing the dependence of the measured thermal effect of dissolution on the ratio of the mass of the salt to the mass of the remote water was obtained (Fig. 39). Another set of samples was prepared to determine the amount of excess water by titrations. From the obtained concentration Cl^- the true concentration of double salt calculated and compared with the mass of salt after drying and the amount of excess water was calculated. Then the amount of excess water was recalculated for those samples for which dissolution enthalpy is known and the dependence of the dissolution enthalpy on the amount of water in the sample was obtained. The equation was determined by Nonlinear curve fitting method and ΔH_{diss}° was calculated for the dry linkage. Its magnitude is $-72 kJ/mol$.

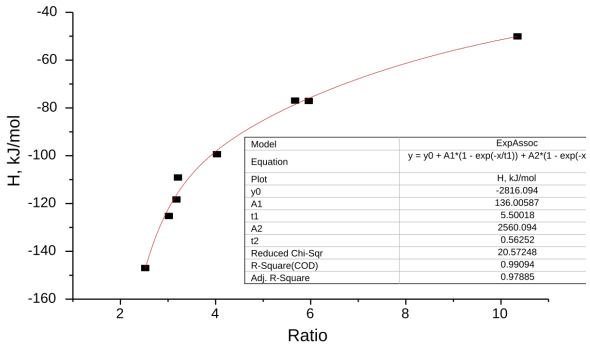

Figure 39. Dependence of the thermal effect on the ratio of the salt mass to the mass of evaporated water.

The mixtures of $MgCl_2 \cdot 6\,H_2O$ and LiCl were prepared from dry compounds in a dry box and then stored in sealed ampoules under vacuum, the probability of absorption water from the air is negligible. The average thermal dissolution effect the salt mixture is $-47kJ/mol$. Figure 40 represents thermochemical cycle for calculation of standard formation enthalpy of the double salt.

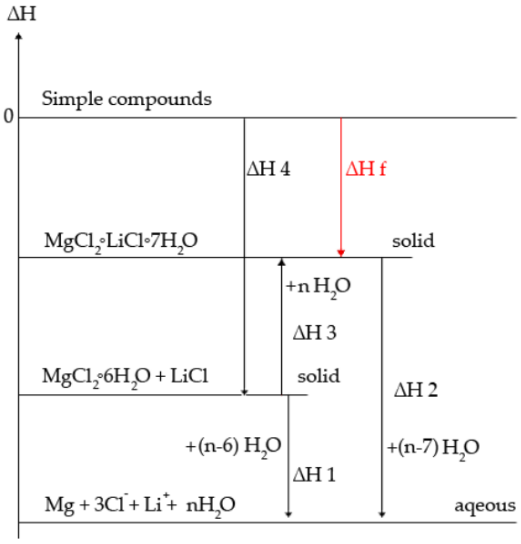

Figure 40. Thermochemical cycle of the system including Mg and Li.

- ΔH_1^∞ is dissolution enthalpy of salt mixture
- ΔH_2^∞ is double salt dissolution enthalpy
- ΔH_3^0 is reaction $[MgCl_2 \cdot 6\,H_2O] + [LiCl] + H_2O = [MgCl_2 \cdot LiCl \cdot 6\,H_2O]$ enthalpy

- ΔH_4^0 is the sum of the standard formation enthalpies [$MgCl_2 \cdot 6\,H_2O$] and [LiCl]
- ΔH_f^0 is the standard formation enthalpy of double salts

For the reaction of the double salt formation from the constituent components the thermal effect can be calculated by the following formula:

$$\Delta H_3^0 = \Delta H_1^0 - \Delta H_2^0 = -47 + 72 = 25 kJ/mol \tag{9}$$

From the literature data [46] ΔH_4^0 can be calculated:

$$\Delta H_4^0 = \Delta H_f^0(\mathrm{MgCl_2 \cdot 6\,H_2O}) + \Delta H_f^0(\mathrm{LiCl}) = -2498.852 + (-408.36) = -2090.49 kJ/mol \tag{10}$$

According to the law of masses it is necessary to take into account that for the formation of a double salt, the components do not have extra water molecule. That is, to ΔH_4^0 you need to add the enthalpy of water formation [47], and get the value is $-2376 kJ/mol$. And the enthalpy of double salt formation can be calculated by the following formula:

$$\Delta H_f^0 = \Delta H_4^0 + \Delta H_3^0 = -2376 + 25 = -2351 kJ/mol \tag{11}$$

4.3.3 $LiCl \cdot 3\,CsCl \cdot 4\,H_2O$

In the work that was made in our laboratory in the last year and was published as a paper [48], the thermal dissolution effects of the double salt $LiCl \cdot 3\,CsCl \cdot 4\,H_2O$ and the mixture of binary salts LiCl, CsCl were also measured. The dissolution enthalpy of the double salt is $+56.85 kJ/mol$, and of the mixture is $+18.6 kJ/mol$. From the Born-Haber cycle the standard formation enthalpy of double salt (Fig. 41) can be calculated with help of Hess law.

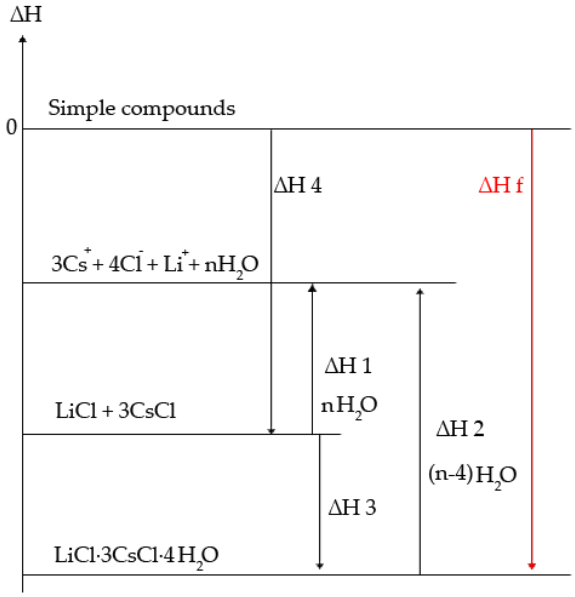

Figure 41. Thermochemical cycle of the system including Li and Cs.

- ΔH_1^{∞} is dissolution enthalpy of salt mixture
- ΔH_2^{∞} is double salt dissolution enthalpy
- ΔH_3^0 is reaction [LiCl] + [CsCl] + 4 H_2O = [$LiCl \cdot CsCl \cdot 4\,H_2O$] enthalpy
- ΔH_4^0 is the sum of the standard formation enthalpies [CsCl] and [LiCl]
- ΔH_f^0 is the standard formation enthalpy of double salts

The reaction enthalpy of the formation of double salts and components are calculated by the formula:

$$\Delta H_3^0 = \Delta H_1^0 - \Delta H_2^0 = -38 kJ/mol \tag{12}$$

One can calculate the formation enthalpy of components, taking into account 4 water molecules present in the double salt:

$$\Delta H_4^0 = 4 \cdot \Delta H_f^0(\mathrm{H_2O}) + 3 \cdot \Delta H_f^0(\mathrm{CsCl}) + \Delta H_f^0(\mathrm{LiCl}) = -2810 kJ/mol \tag{13}$$

The standard formation enthalpy of double salt can be calculated by equation:

$$\Delta H_f^0 = \Delta H_4^0 + \Delta H_3^0 = -2848 kJ/mol \tag{14}$$

The table 16 shows the calculated ΔH_f^0, kJ/mol for double salts.

Table 16. Standard formation enthalpy of double salts.

Double salt	ΔH_f^0, kJ/mol
$MgCl_2 \cdot LiCl \cdot 7\,H_2O$	-2351
$MgCl_2 \cdot CsCl \cdot 6\,H_2O$	-2831
$LiCl \cdot 3\,CsCl \cdot 4\,H_2O$	-2848

One can't help but notice the fact that in the case of $MgCl_2 \cdot LiCl \cdot 7\,H_2O$ and $MgCl_2 \cdot CsCl \cdot 6\,H_2O$ double salts the thermal formation effects from mixtures of compounds are positive, it means that the reaction occurs with heat absorption. It was possible to confirm experimentally and it has been shown in the literature [49], [50], that double salts are forming in ternary systems and this reaction is not always exothermic, one may assume that the entropic factor plays a main role in the formation of a double salt. Using the ΔG at T=298 K taken from literature data [51], we can exactly calculate the entropy factor of the reaction of the double salt formation from simple salts. The magnitudes of the entropy change are presented in table 17.

Table 17. Calculated entropy factors for the formation of double salts from simple mixture.

Double salt	ΔS, J/mol $\cdot$ K
$MgCl_2 \cdot LiCl \cdot 7\,H_2O$	9.46
$MgCl_2 \cdot CsCl \cdot 6\,H_2O$	40.50

As you can see, the biggest entropy factor is obtained for the salt $MgCl_2 \cdot CsCl \cdot 6\,H_2O$. This can be explained by its structure according to XRC data. As it was mentioned earlier, in the process of double salt formation the structures of magnesium crystallohydrate and anhydrous cesium chloride are barely changing. The solid macrophase (single crystal) consists of two microphases. It is a combination of two microphases and it creates a large entropy factor. Comparison with salts $LiCl \cdot 3\,CsCl \cdot 4\,H_2O$ and $MgCl_2 \cdot LiCl \cdot 7\,H_2O$ allows to understand this process. Salt $LiCl \cdot 3\,CsCl \cdot 4\,H_2O$ has a small entropy factor, but in its structure there are big changes in symmetry and in the spatial arrangement of ions relative to each other. Generally the structure is formed by mutual changes in substructures and their adjustment, formation of the general and common system of bonds. For the structure $MgCl_2 \cdot LiCl \cdot 7\,H_2O$ the entropy factor is also large. According to crystal structure, it can be said that in this case lithium and his entourage penetrate into the substructure, organized by the magnesium and environment, which in the considered cases

remains practically unchanged. Naturally, such integration must change the characteristic of the spatial environment.

4.4 NMR

4.4.1 Spectroscopy

NMR spectra on the ^{133}Cs nucleus were obtained for concentrated solution m(LiCl)=10 mol/kg, m(CsCl)=5 mol/kg at room temperature 278 K (Fig. 42). For this concentration according to the cryoscopic experiment the freezing temperature is below 278 K. Two peaks were determined on spectra at nucleus ^{133}Cs. This phenomenon was discovered previously, we were able to confirm its existence and results reproducibility. Based on the findings of previous experiments, we can conclude the presence of long-living microphases containing Cs, involved in slow chemical exchange. Moreover, the two peaks carry information about the different environment of cesium in microphases. Thus the existence of microheterogeneity in the concentrated solution systems $LiCl-CsCl-H_2O$ is confirmed.

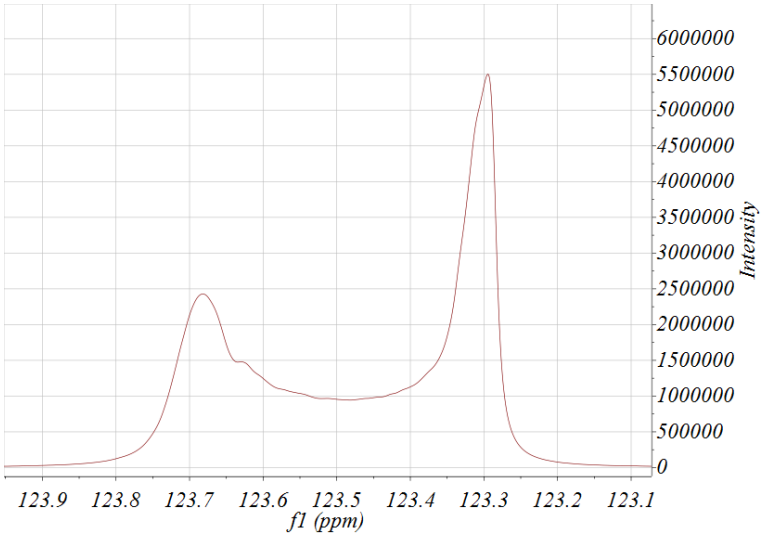

Figure 42. Two peaks on ^{133}Cs nucleus.

4.4.2 Self-diffusion of water molecules

Figures 43 and 44 show the dependence of the relative self-diffusion coefficient of water at 298 K on LiCl and $MgCl_2$ concentrations in $LiCl-MgCl_2-H_2O$ system. Relative self-

diffusion coefficients were calculated for each concentration $D(^1H)_{solution}/D(^1H_{water})$. The curve trace demonstrates the cumulative effect of the kosmotropic ions Li^+ and Mg^{2+} on the mobility of water molecules. Immediately after adding a small amount of salt a sharp inhibition of water molecules motion, obviously, in consequence of the fact that the water begins to be structurized around ions, hydrate them. Compared to binary systems [52] the abrupt inhibition of water molecules in the ternary system is particularly noticeable. Like it was expected from cryoscopic data in the system there is an area of glazing, which reflects the competition between ions for water molecules. Thus, the ions Li^+ and Mg^{2+} affect each other and water molecules, reducing its mobility.

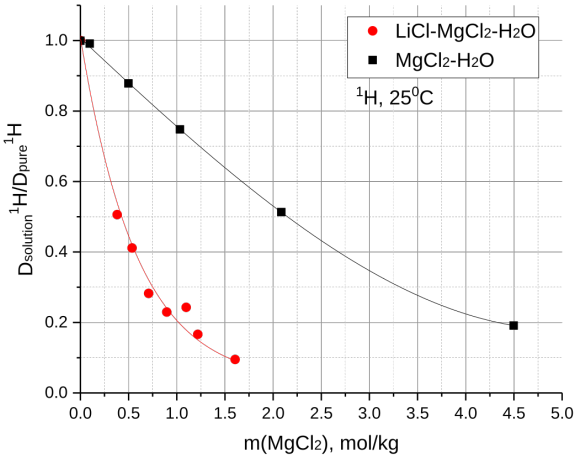

Figure 43. Dependence of relative self-diffusion coefficients on concentration $MgCl_2$ for double and ternary systems.

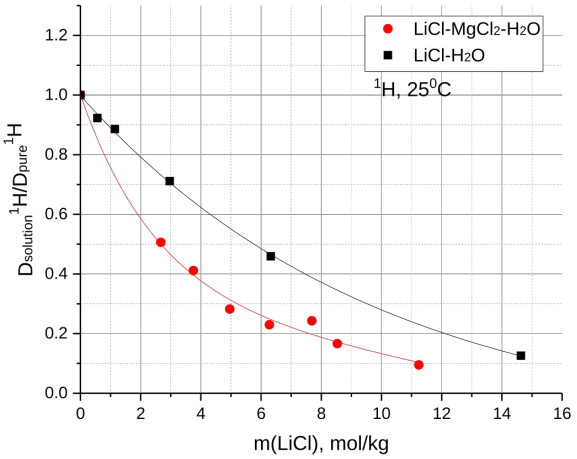

Figure 44. Dependence of relative self-diffusion coefficients on LiCl concentration for double and ternary systems.

In a concentrated solution of the ternary system it is seen that the self-diffusion coefficient of water molecules is comparable in value with that in concentrated solutions of double systems. Under the assumption that at such high salt concentrations there are not enough water molecules for hydration of both ions, and between Mg and Li there is competition, according to the XRC data the water molecules enter the octahedral environment of Mg, and in the tetrahedral environment of Li there is only one water molecule, Li clearly loses to Mg. Also in solution, water molecules mainly hydrate Mg and, basically their mobility in the first approximation is similar to that in the dual system $MgCl_2 - H_2O$. Then, Li is responsible for additional braking observed. This approximation can be considered only at the qualitative level, since, of course, neither the Mg octahedra nor the Li tetrahedra are isolated in the solution and have a direct effect on each other, especially since both seek to coordinate water molecules around themselves. Thus, lithium and magnesium mutually enhance the inhibition of the mobility of water molecules.

Figure 45 shows the dependence of the self-diffusion coefficient of water molecules on the total concentration Cl^- in the system $LiCl - CsCl - H_2O$. In this case, the curve can be divided into two sections: flat up to 5 mol/kg (LiCl); 2.5 mol/kg (CsCl) and inclined.

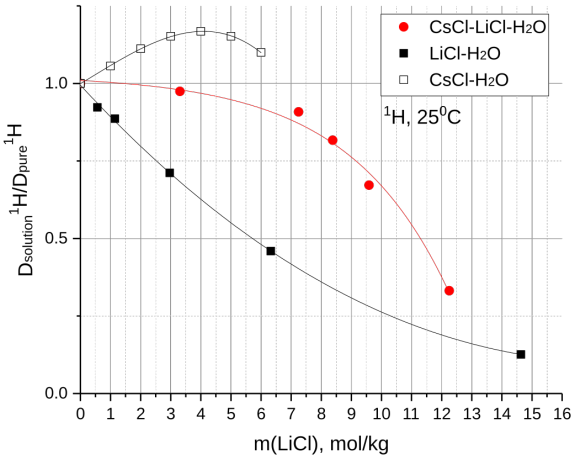

Figure 45. Concentration dependence of relative self-diffusion rates.

After the concentration of m(Cl−) 7.5 mol/kg there is a sharp inhibition of water molecules. Eutectic concentration was determined to be ~7mol/kg (Cl^-) according to the results of cryoscopic studies. The sharp decrease of the self-diffusion coefficient after eutectic concentration can be associated with the restructuring of the solution, a sharp change in the dominant structure. Especially in the presence of micro-uniformity in the post-eutectic region in this system. Turning to the data of the XRC, we note that

in this system, in the most concentrated solution, Li is surrounded mainly by the water molecules. This thesis finds confirmation in the fact that in solutions of pre-eutectic concentrations Cs ion is hydrated and that it is clearly reflected on the average magnitude of water molecules self-diffusion coefficients. Cs is a chaotropic ion and increases the water molecules mobility in its immediate environment.

Figures (Fig. 46 and 47) show the dependences of the water molecules self-diffusion coefficients for the ternary system $MgCl_2 - CsCl - H_2O$ on the concentrations $MgCl_2$ and CsCl along with water molecules self-diffusion coefficients in binary systems [52]. In this case, unlike previous systems, the dependence is almost linear. In this system, there is no sharp adjustment of the solution with an increase in concentration or competition for water molecules between the strongly kosmotropic Mg and the chaotropic Cs. The system smoothly and gradually changes its dominant structure with increasing concentration. According to XRC there is no noticeably strong disturbance of the crystal structures of Mg or Cs compared to simple binary salts, and the water molecules in the solid phase are coordinated around Mg solely.

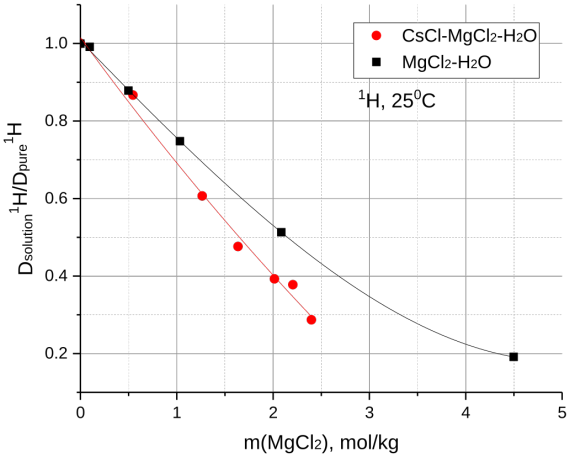

Figure 46. The dependence of the relative self-diffusion coefficients from the total concentration $MgCl_2$.

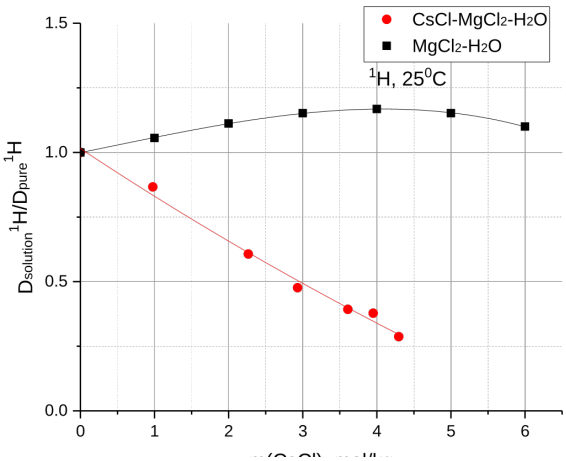

Figure 47. The dependence of the relative self-diffusion coefficients on the concentration of CsCl in double and ternary systems.

Let us stop at the first remark and consider the linear dependence, for this system we could not reach the high concentrations region, we do not obtain the values of the self-diffusion coefficients for the post-eutectic region. Weak deviations from the symmetry of the environment, the distances to the nearest atoms and the preservation of angles for both Mg and Cs, as well as the high formation entropy of a double salt $MgCl_2 \cdot CsCl \cdot H_2O$ from binary salts and crystallohydrates give the right to state that there are favorable conditions for the restructuring of the solution and a smooth, unimpeded change of the solvent from water to another dominant structure. In this system, there are no anomalies such as the glass transition of the solution or the region of metastability according to polythermal measurements, as mentioned earlier. Given the fact that water molecules in the solid phase are coordinated exclusively around magnesium, we assume that the decrease in the mobility of water molecules is due to their coordination around magnesium and in the solution too, and in the ternary system this effect is more active than in the binary system. This interesting phenomena can be explained by the fact that in the CsCl (according to XRC) tends to form associates. The formation of such associates affects the Mg^{2+} environment so that it removes Cl from the second solvating Mg shell. Since Mg forms crystallohydrates of type $MgCl_2 \cdot 8\,H_2O$ and $MgCl_2 \cdot 12\,H_2O$, where water molecules are coordinated around Mg, forming an octahedron, and are additionally coordinated around this octahedron. Thus, the association of Cs with Cl enables $Mg(H_2O)_6$ to coordinate additional water molecules and create their additional inhibition. Since, as mentioned above, the area of post-eutectic concentrations is not achieved, interpretation of the data does not operate with such concepts as CG. Nevertheless, we know that the restructuring of this solution with increasing concentrations occurs smoothly, and magnesium is much better hydrated than cesium. In

this case, we can speak about the creation of favorable conditions for deceleration of the water molecules in the second hydration sphere of the magnesium.

4.4.3 Longitudinal relaxation times T_1

In the previous work the relaxation times were measured at the nuclei ^{133}Cs in $LiCl-CsCl-H_2O$ system at wide concentration and temperature ranges. In this work, the same measurements were performed for the system $MgCl_2-CsCl-H_2O$. Comparative relaxation times are shown in figure 48. ^{133}Cs is a quadrupole nuclei, and the main mechanism of its relaxation is quadrupole [53]. The rate of longitudinal relaxation is determined by the following ratio:

$$1/T_1 = A\Big(\frac{e^2qQ}{\hbar}\Big)^2\Big(\frac{\tau_\theta}{1+\omega_0^2\tau_\theta^2} + \frac{4\tau_\theta}{1+4\omega_0^2\tau_\theta^2}\Big) \tag{15}$$

Where A is the coefficient characteristic of each nuclei, τ_θ - corelation time, ω_0 - resonance frequency. This formula is true in conditions of isotropic fluid motion and uniqueness exponential function of free induction decay. Quadrupole coupling constant (QCC) $e^2qQ/\hbar$ along with correlation time determine the relaxation rate of the quadrupole nucleus. QCC directly depends on the symmetry of the nearest nucleus environment, the electric field gradient (EFG). Whereas the correlation time is determined by the mobility of this environment and characterizes the spectral fluctuations density of the EFG at the resonance frequency during the exponential decay of the corresponding correlation function. For this solutions we didn't manage to reach the dispersion region and all measurements were conducted for the area of maximum contraction, it was not possible to determine the QCC or correlation time, however, we can state that correlation times are small because the area of maximum contraction corresponds to $\omega\tau << 1$, that is, the mobility of the nearest the environment of cesium is large and decreases with increasing concentration and decreasing temperatures.

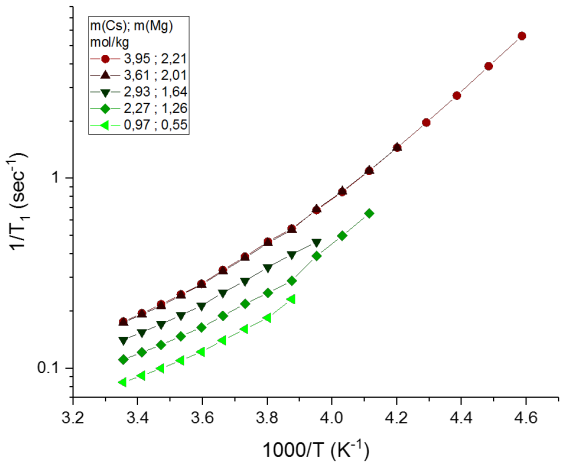

Figure 48. Temperature dependence of relaxation rates on the nucleus ^{133}Cs.

The figure 48 shows the dependence of the longitudinal relaxation rate in the coordinates of the natural logarithm on the inverse temperature for $CsCl-MgCl_2-H_2O$ system. It is noticeable that at 273K dependence deviates from linearity, then in the range of 298-273K of "high" temperatures where the dependence is linear the activation energy of relaxation processes can be estimated. According to the modified Arrhenius equation, relation between the relaxation rate and the activation energy is set by the following ratio:

$$1/T_1 = A\tau_0 \exp\left(E_a/RT\right) \tag{16}$$

Then, the slope of the logarithmic dependence relaxation rates from the reverse temperature was determined, and the activation energies of relaxation ^{133}Cs in $LiCl-CsCl-H_2O$ system and $MgCl_2-CsCl-H_2O$ in solutions of different concentrations were calculated. Data is shown in figure 49. It should be noted that after 273K there is a noticeable deviation from the linear dependence. If QCC remains constant throughout the temperature range, the activation energy of relaxation processes increases with decreasing temperatures.

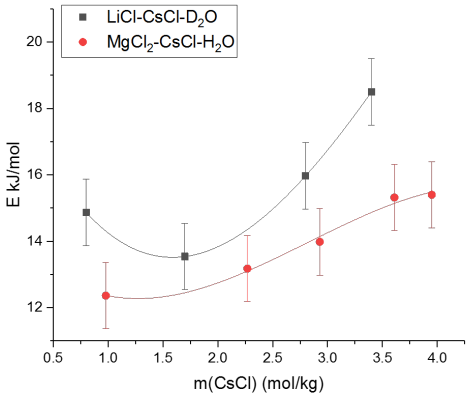

Figure 49. Comparison of concentration dependencies of activation energy for ternary systems.

Cesium has a large radius and a single positive charge Cs^+, so it is a chaotropic ion. Mainly in solutions of high concentrations cesium forms ion pairs, as it has been shown previously, it is reflected in the properties and characteristics of concentrated solutions. To sum up, cesium has the tendency to form micro domains in solutions with its own quasi-crystalline lattice. Increase in activation energies with increasing salts concentration indicates an increase in the potential barrier of the ^{133}Cs relaxation process.

5 Conclusions

1. For the first time, the double salt of $4\,LiCl \cdot 3\,CsCl \cdot 2\,H_2O$ was extracted, its structure was characterized by the XRC method.

2. Standard formation enthalpies of double salts were determined for the first time.

3. It was shown that the formation of the double salt $LiCl \cdot 3\,CsCl \cdot 4\,H_2O$ is driven by the enthalpy factor, and the formation of the salts $LiCl \cdot MgCl_2 \cdot 7\,H_2O$ and $MgCl_2 \cdot CsCl \cdot 6\,H_2O$ by the entropy factor.

4. The tendency of Cs^+ to organize its own sub-structure is manifested in the water molecules mobility reduction in systems containing chlorides of Li and Mg.

5. The effect of Mg^{2+} and Cs^+ cations on Li^+ was found. This is expressed in the variability of Li^+ closest environment in solutions and in the solid phase.

REFERENCES

[1] Georgios M. Kontogeorgis, Bjørn Maribo-Mogensen, and Kaj Thomsen. The debye-hückel theory and its importance in modeling electrolyte solutions. *Fluid Phase Equilibria*, 462:130 – 152, 2018.

[2] J Barthel, W Kunz, and R Neueder. Electrolyte Solutions, Thermodynamics. In Robert A Meyers, editor, *Encyclopedia of Physical Science and Technology (Third Edition)*, pages 219–241. Academic Press, New York, third edit edition, 2003.

[3] Qi Dong, Xiahui Yao, Yanyan Zhao, Miao Qi, Xizi Zhang, Hongyu Sun, Yumin He, and Dunwei Wang. Cathodically Stable Li-O2 Battery Operations Using Water-in-Salt Electrolyte. *Chem*, 4(6):1345–1358, 2018.

[4] Liumin Suo, Oleg Borodin, Tao Gao, Marco Olguin, Janet Ho, Xiulin Fan, Chao Luo, Chunsheng Wang, and Kang Xu. Water-in-salt electrolyte enables high-voltage aqueous lithium-ion chemistries. *Science*, 350(6263):938–943, 2015.

[5] Vladimir Majer, Josef Sedlbauer, and Robert H Wood. Calculation of standard thermodynamic properties of aqueous electrolytes and nonelectrolytes. In *Aqueous Systems at Elevated Temperatures and Pressures*, pages 99–147. Elsevier, 2004.

[6] Alexander Zhdanovskyi. *Multi-component water-salt systems solubility experimental data*. GosKhimIzdat, Leningrad, Moscow, 1 edition, 1973.

[7] Reham M. Abu Shmeis. Chapter one - water chemistry and microbiology. In Dotse Selali Chormey, Sezgin Bakrdere, Nouha Bakaraki Turan, and Güleda Önkal Engin, editors, *Fundamentals of Quorum Sensing, Analytical Methods and Applications in Membrane Bioreactors*, volume 81 of *Comprehensive Analytical Chemistry*, pages 1 – 56. Elsevier, 2018.

[8] R.A. Robinson and R.H. Stokes. *Electrolyte Solutions: Second Revised Edition (Dover Books on Chemistry)*. Dover Publications, 2002.

[9] P.A. Alcântara Pessôa Filho, G.A. Medeiros Hirata, É.O. Watanabe, and É.A. Miranda. 2.46 - precipitation and crystallization. In Murray Moo-Young, editor, *Comprehensive Biotechnology (Second Edition)*, pages 651 – 663. Academic Press, Burlington, second edition edition, 2011.

[10] O.N. Pestova, V.E. Baranauskaite, and M.K. Khripun. Formation of binary salts in the system LiClCsClH2O. *Russian Journal of General Chemistry*, 86(4), 2016.

[11] O. N. Pestova, L. A. Myund, M. K. Khripun, Yu. P. Kostikov, and A. A. Proyavkin. Structural microheterogeneites in strontium perchlorate solutions of posteutectic concentrations. *Russian Journal of General Chemistry*, 78(7):1295–1299, jul 2008.

[12] Hydrogen. In Greenwood N.N and Earnshaw A., editors, *Chemistry of the Elements (Second Edition)*, pages 32–67. Butterworth-Heinemann, Oxford, second edi edition, 1997.

[13] J L Finney. Ice: Structures. In *Reference Module in Materials Science and Materials Engineering*, pages –. Elsevier, 2016.

[14] M J Calhorda and P J Costa. 9.12 - Weak Hydrogen Bonding. In Jan Reedijk and Kenneth Poeppelmeier, editors, *Comprehensive Inorganic Chemistry {II} (Second Edition)*, pages 341–357. Elsevier, Amsterdam, second edi edition, 2013.

[15] Alan K Soper. Chapter 3 - The Structure of Water and Aqueous Systems. In Felix Fernandez-Alonso and David L Price, editors, *Neutron Scattering - Applications in Biology, Chemistry, and Materials Science*, volume 49 of *Experimental Methods in the Physical Sciences*, pages 135–211. Academic Press, 2017.

[16] Henry S. Frank and Wen-Yang Wen. Ion-solvent interaction. structural aspects of ion-solvent interaction in aqueous solutions: a suggested picture of water structure. *Discuss. Faraday Soc.*, 24:133–140, 1957.

[17] M. K. Khripun, A. A. Kiselev, and S. V. Zubtsov. Comparative analysis of the solubility of alkali metal chlorides in cadmium and zinc nitrate solutions at 25c. *Russian Journal of General Chemistry*, 74(6):834–837, jun 2004.

[18] Khripun M.K. Lilich L.S. *Rastvory kak himicheskie sistemy [In Russian]*. SPbSU, 2010.

[19] Mingjun Yang, Zheng Rong Chong, Jianan Zheng, Yongchen Song, and Praveen Linga. Advances in nuclear magnetic resonance (nmr) techniques for the investigation of clathrate hydrates. *Renewable and Sustainable Energy Reviews*, 74:1346 – 1360, 2017.

[20] N.S. Sullivan. Nuclear magnetic resonance studies of tunneling in quantum solids at very low temperatures. *Progress in Nuclear Magnetic Resonance Spectroscopy*, 90-91:74 – 91, 2015.

[21] C. Griesinger, M. Bennati, H.M. Vieth, C. Luchinat, G. Parigi, P. Höfer, F. Engelke, S.J. Glaser, V. Denysenkov, and T.F. Prisner. Dynamic nuclear polarization at high

magnetic fields in liquids. *Progress in Nuclear Magnetic Resonance Spectroscopy*, 64:4 – 28, 2012.

[22] Vladimir I. Chizhik, Andrei V. Egorov, Maria S. Pavlova, Maria I. Egorova, and Aleksey V. Donets. Structure of hydration shell of calcium cation by NMR relaxation, car-parrinello molecular dynamics and quantum-chemical calculations. *Journal of Molecular Liquids*, 224:730–736, dec 2016.

[23] E.A. Krylova, M.G. Shelyapina, P. Nowak, H. Harańczyk, M. Chislov, I.A. Zvereva, A.F. Privalov, M. Becher, M. Vogel, and V. Petranovskii. Mobility of water molecules in sodium- and copper-exchanged mordenites: Thermal analysis and 1 h NMR study. *Microporous and Mesoporous Materials*, 265:132–142, jul 2018.

[24] Timothy D.W. Claridge. Diffusion nmr spectroscopy. In *High-Resolution NMR Techniques in Organic Chemistry*, pages 303–334. Elsevier, 2009.

[25] Peter Stilbs. Diffusion studied using nmr spectroscopy. In *Encyclopedia of Spectroscopy and Spectrometry*, pages 423–428. Elsevier, 1999.

[26] Hermann Weingartner. Nmr studies of ionic liquids: Structure and dynamics. *Current Opinion in Colloid Interface Science*, 18(3):183–189, jun 2013.

[27] J Barthel, W Kunz, and R Neueder. Electrolyte Solutions, Thermodynamics. In Robert A Meyers, editor, *Encyclopedia of Physical Science and Technology (Third Edition)*, pages 219–241. Academic Press, New York, third edit edition, 2003.

[28] I.V. Pobelov. Thermodynamics of ions in solutions. In *Reference Module in Chemistry, Molecular Sciences and Chemical Engineering*. Elsevier, 2017.

[29] H. Gmati-Ben Khaled, I. Khattech, and M. Jemal. Standard molar enthalpy of formation of rubidium diphosphate. *Journal of Thermal Analysis and Calorimetry*, 118(1):579–583, aug 2014.

[30] You-Ying Di, Yu-Han Zhang, Yu-Xia Kong, and Chun-Sheng Zhou. Crystal structure and thermochemistry of anhydrous potassium 2-pyrazine carboxylate (c5h3kn2o2). *Journal of Thermal Analysis and Calorimetry*, 124(3):1545–1553, feb 2016.

[31] A.V. Kustov, O.A. Antonova, N.L. Smirnova, A.A. Kladiev, A.A. Kladiev, T.V. Kudayarova, M.S. Gruzdev, and D.B. Berezin. The energetics of solvation and ion-ion interactions in prospidium chloride aqueous solutions. *Journal of Molecular Liquids*, 263:49–52, aug 2018.

[32] V.G. Lavrent'eva A.N. Kirgintsev, L.N. Trushnikova. *Rastvorimost' Neorganicheskikh Veshchestv V Vode (Solubility of Inorganic Substances in Water)*. Leningrad: Khimiya, 1972.

[33] R.E. Shleymovich A.B. Zdanovskiy, E.I. Lyakhovskaya. *Spravochnik eksperimentalnykh dannykh po rastvorimosti mnogokomponentnykh vodno-solevykh sistem. (Handbook of experimental data on the solubility of multicomponent water-salt systems.)*. Leningrad: Khimiya, 1975.

[34] Yanat'eva Voskresenskaya. *Russian Chemical Bulletin*, 1(1):111–113, 1937.

[35] Lavrent'eva V.G. Kirgintsev A.N., Trushnikova L.N. *Rastvorimost' Neorganicheskikh Veshchestv V Vode (Solubility of Inorganic Substances in Water) [In Russian]*. Leningrad: Khimiya, 1972.

[36] Vaisvel'd Shevchuk. *Inorganic Chemistry Journal*, 12(9):2499, 1967.

[37] V. P. Blidin. Heterogenrous equilibria in the systems LiCl-RbCI-h2o, and LiCI-CsCI-h2o. *Bulletin of the Academy of Sciences of the USSR Division of Chemical Science*, 2(5):723–726, 1954.

[38] O. N. Pestova, V. E. Baranauskaite, and M. K. Khripun. Formation of binary salts in the system LiCl–CsCl–h2o. *Russian Journal of General Chemistry*, 86(4):767–770, apr 2016.

[39] E. Weiss. Die kristallstruktur des lithiumjodid-monohydrats. 341(3-4):203–206, dec 1965.

[40] Julia Sohr, Horst Schmidt, and Wolfgang Voigt. Higher hydrates of lithium chloride, lithium bromide and lithium iodide. *Acta Crystallographica Section C Structural Chemistry*, 74(2):194–202, jan 2018.

[41] Erik Hennings, Horst Schmidt, and Wolfgang Voigt. Crystal structures of hydrates of simple inorganic salts. II. water-rich calcium bromide and iodide hydrates: CaBr2·9h2o, CaI2·8h2o, CaI2·7h2o and CaI2·6.5h2o. *Acta Crystallographica Section C Structural Chemistry*, 70(9):876–881, aug 2014.

[42] Kunihisa Sugimoto, Robert E. Dinnebier, and Jonathan C. Hanson. Structures of three dehydration products of bischofite fromin situsynchrotron powder diffraction data mgcl2*nh2o, n=1,2,4. *Acta Crystallographica Section B Structural Science*, 63(2):235–242, mar 2007.

[43] R. W. G. Wyckoff. Cscl structure, cesium chloride structure. *Crystal Structures*, 1:85–237, 1963.

[44] C. Howard Shomate and Eugene H. Huffman. Heats of formation of MgO, MgCl2, MgCl2·h2o, MgCl2·2h2o, MgCl2·4h2o, and MgCl2·6h2o1. *Journal of the American Chemical Society*, 65(8):1625–1629, aug 1943.

[45] Gerald K Johnson and Karl H Gayer. The enthalpies of solution and formation of the chlorides of cesium and rubidium. *The Journal of Chemical Thermodynamics*, 11(1):41 – 46, 1979.

[46] Vivian B Parker. *Thermal Properties of Aqueous llni-univalent Electrolytes*. U. S. Govt. Printing Office, Washington, D. C., 1965.

[47] F.D. Rossini. The heat of formation of water. *Bureau of Standards Journal of Research*, 6(1):1, jan 1931.

[48] Kondrat'ev YU.V. Pestova O. N. Bukesova V. A. Khripun V. D. Baranauskaite V. E. Energetic properties of dissolution processes of double salt licl and cscl in water. *Journal of Inorganic Chemistry*, 88(3):506–507, 2018.

[49] J Braunstein. Some aspects of solution chemistry in liquid mixtures of inorganic salts with water. *Inorganica Chimica Acta Reviews*, 2:19 – 30, 1968.

[50] Zhihong Liu, Jingchao Chai, Gaojie Xu, Qingfu Wang, and Guanglei Cui. Functional lithium borate salts and their potential application in high performance lithium batteries. *Coordination Chemistry Reviews*, 292:56 – 73, 2015.

[51] Mikhail Skripkin. Interaction and mutual influence of the components in the systems mgcl2-mcl-h2o (m=li-cs, nh4) [in russian]. *Dissertation, Leningrad*, page 105, 1990.

[52] Self-diffusion data for binary aqueous electrolyte solutions. In R. Mills and V.M.M Lobo, editors, *self-diffusion in electrolyte solutions*, volume 36 of *Physical Sciences Data*, pages 19 – 254. Elsevier, 1989.

[53] Wayne J. DeWitte, Richard C. Schoening, and Alexander I. Popov. Cesium-133 nmr studies of cs+ salts in various solvents. *Inorganic and Nuclear Chemistry Letters*, 12(3):251 – 253, 1976.